Earth and Planetary Science Letters 594 (2022) 117694

Contents lists available at ScienceDirect

Earth and Planetary Science Letters

www.elsevier.com/locate/epsl

# Tridymite in a lacustrine mudstone in Gale Crater, Mars: Evidence for an explosive silicic eruption during the Hesperian

V. Payré [a,b,*], K.L. Siebach [b], M.T. Thorpe [b,c], P. Antoshechkina [d], E.B. Rampe [c]

[a] Department of Astronomy and Planetary Science, Northern Arizona University, 527 South Beaver Street, Flagstaff, AZ 86011-6010, United States of America
[b] Department of Earth, Environmental, and Planetary Sciences, Rice University, 6100 Main Street, Houston, TX 77005, United States of America
[c] Astromaterials Research and Exploration Science Division, NASA Johnson Space Center, Houston, TX 77058, United States of America
[d] Division of Geological and Planetary Sciences, California Institute of Technology, 1200 East California Boulevard, Pasadena, CA 91125, United States of America

ARTICLE INFO

*Article history:*
Received 30 April 2021
Received in revised form 13 June 2022
Accepted 23 June 2022
Available online 19 July 2022
Editor: W.B. McKinnon

*Keywords:*
silicic explosive eruption
Gale crater lake
Mars
Hesperian
tridymite
felsic magmatism

ABSTRACT

The unexpected detection of ∼16 wt.% monoclinic tridymite, a high-temperature silica polymorph, within an otherwise lacustrine mudstone in Gale crater, Mars raises significant questions about its formation and the extent of magmatic evolution on that planet. The rock sample, analyzed by the X-ray diffractometer onboard the *Curiosity* rover, also contained feldspar, cristobalite, and opaline silica (±Si-glass). Monoclinic tridymite is extremely rare on Earth, and has only been discovered in silicic volcanic environments, high-temperature impact settings, and extraterrestrial rocks. We review the most common formation pathways of natural tridymite and run thermodynamical models to investigate possible formation mechanisms. We consider the broader context of the sample to propose a formation and transport mechanism based on: (1) the mineralogical assemblage of the mudstone and rocks in the vicinity, (2) the composition of the mudstone layer, and (3) the overall geological context. Based on the large amount of tridymite, the high $SiO_2$ and low $Al_2O_3$ concentration of the mudstone, and the low temperature context within distal lacustrine mudstone, we propose that an explosive eruption released Si-rich ashes, which were deposited into Gale crater's watershed as a tridymite-rich ashfall along with cristobalite, feldspar, Ti-oxide, and Si-rich glass, when Gale was still a lake (Hesperian). The dissolution of Si-rich glass and mineral sorting during transport would have concentrated tridymite, caused opaline silica precipitation, and relatively lowered the $Al_2O_3$ concentration. This scenario implies that explosive volcanism on Mars occurred during the Hesperian and might not be restricted to basaltic eruptions, revealing the complexity of Mars magmatism.

© 2022 The Authors. Published by Elsevier B.V. This is an open access article under the CC BY-NC license (http://creativecommons.org/licenses/by-nc/4.0/).

## 1. Introduction

The Gale impact crater, which formed a sedimentary basin on Mars ∼3.7-3.0 Ga, contains an exposed interval of >380 m of dominantly lacustrine strata described as the Murray formation that has been investigated by the Mars Science Laboratory *Curiosity* rover. The majority of the rocks contain detrital pyroxenes, ∼48-52 wt.% $SiO_2$ and <1 wt.% crystalline silica, strong indications that the provenance terrains exposed around the crater and in the crater walls are largely basaltic. A single 1-m thick interval of lacustrine strata (Czarnecki et al., 2020a) sampled with the "Buckskin" drill sample, contained 73.9 wt.% $SiO_2$, including 15.6 wt.% crystalline monoclinic tridymite, 2.6 wt.% cristobalite, and ∼54 wt.% high-Si amorphous material, with plagioclase, and minor magnetite (detection limit for crystalline minerals is 1 wt.%).

The unique composition and mineralogy of the Buckskin sample and high-silica interval inspired a series of publications and hypotheses about its origin. Tridymite is a high-temperature, low-pressure polymorph of $SiO_2$ and was quickly recognized as a likely strong indicator of silicic volcanism, thought to be exposed in the rocks of the crater walls or central peak (Morris et al., 2016). Subsequent papers noted that the high silica layer could represent more distal lake deposits of a redox-stratified lake, where mineral sorting and redox conditions conspired to deposit amorphous silica and magnetite (Hurowitz et al., 2017) or the high silica may have been left behind by minor acidic diagenesis (Rampe et al., 2017). Recent work has suggested the measured locale could have formed from a hydrothermal fumarolic deposit (Yen et al., 2021). Understanding the formation and transport of tridymite has crucial

* Corresponding author.
*E-mail address:* valerie.payre@nau.edu (V. Payré).

https://doi.org/10.1016/j.epsl.2022.117694
0012-821X/© 2022 The Authors. Published by Elsevier B.V. This is an open access article under the CC BY-NC license (http://creativecommons.org/licenses/by-nc/4.0/).

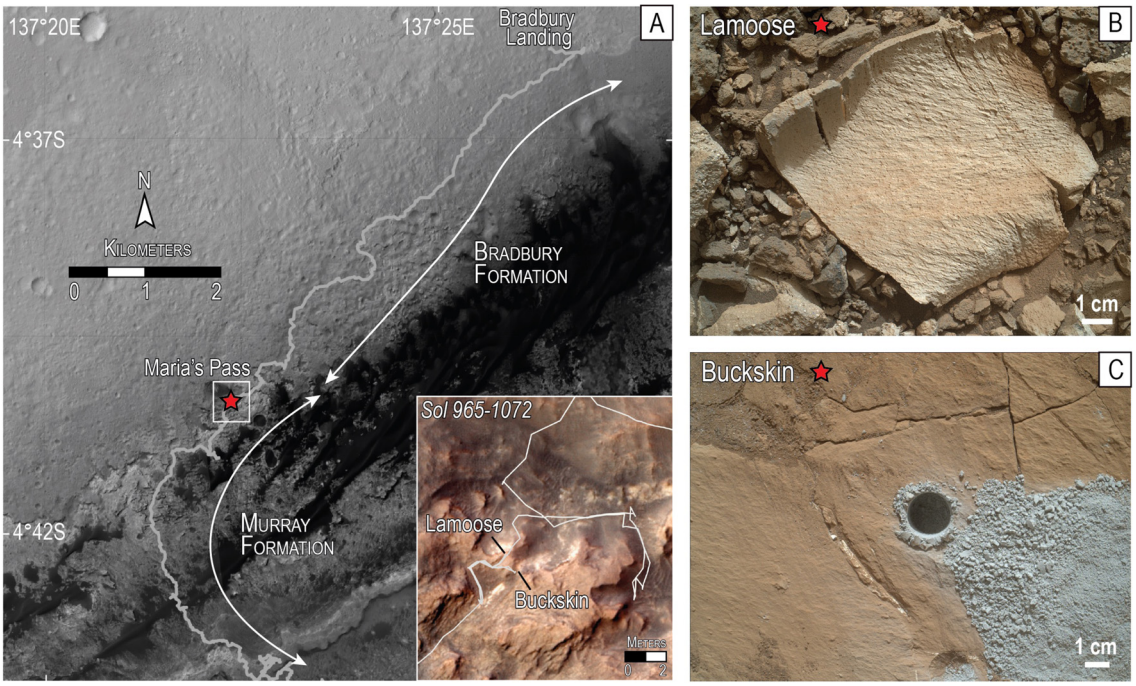


**Fig. 1.** (a) Curiosity traverse with the Bradbury Landing and Maria's Pass waypoints indicated. The red star shows the location of the Buckskin mudstone sample, and the Bradbury and Murray formation are indicated for reference. An inset of Maria's Pass is showed on the bottom right. Credit: NASA/JPL-Caltech/Univ. of Arizona. (b-c) Images from the Mars Hand Lens Imager onboard the Curiosity rover of (b) Lamoose, a local float block adjacent to Buckskin within the Murray formation showing laminations, and (c) Buckskin.

geological implications regarding the environmental conditions at the time of its deposition.

In this manuscript, we revisit the mineralogical and sedimentological data at/around the Buckskin drill site, with particular emphasis on terrestrial analogs for monoclinic tridymite and the recognition that this interval is unique in hundreds of meters of lacustrine stratigraphy. We ultimately concur with Morris et al. in the silicic volcanism scenario for forming monoclinic tridymite and introduce thermodynamical models showing that tridymite is a reasonable product of evolution of the same magmatic processes that produced other source rocks to Gale crater. The monoclinic form of tridymite is most consistent with an ashy eruption but not with a direct ashfall because $Al_2O_3$ is too low for rhyolitic glass, and no unconformities or changes in sedimentation style consistent with a direct ashfall from a novel source were observed. Given these observations and the purity of the single pulse of tridymite and high-$SiO_2$ in hundreds of meters of lacustrine stratigraphy, we propose that the observations are most consistent with a syndepositional ashy rhyolitic eruption that would have introduced an abundance of fine grained tridymite-rich material to the watershed of Gale crater, suggesting that a felsic explosive eruption occurred during the Hesperian. The Buckskin sample would be a distal lacustrine deposit, enriched in tridymite through sorting and in $SiO_2$ through precipitation. An analogous site at Lake Tecocomulco, Mexico demonstrates the feasibility of such a scenario, with a ∼2 m thick layer of lacustrine deposits enriched in tridymite and $SiO_2$ but depleted in $Al_2O_3$ and mafic minerals after an ashy rhyolitic eruption ∼60 km away (presumably Tláloc volcano; Roy et al., 2009a,b).

## 2. Tridymite detection in Gale crater

### 2.1. Geologic context

The *Curiosity* rover landed in the 3.8 Ga Gale impact crater, which contains a wind-exposed stratigraphic record in the form of a central mound called Aeolis Mons (Fig. 1). The lower part of the mound contains layered hydrated minerals that the rover was sent to investigate. The uppermost few kilometers of the mound have been proposed to come from volcanic or eolian activity, and are likely wind-blown dust or ash deposits (Thomson et al., 2019; Kite et al., 2013; Thomson et al., 2011). Textural similarities and low thermal inertia of the uppermost central mound and the Medusae Fossae Formation, thought to be a volcanic ash deposit and a large source of dust located ∼400 km east of Gale crater, suggest that volcanic ash may have contributed to building the central mound (Thomson et al., 2011).

During the first 750 martian days (known as sols), the rover traveled through fluvio-deltaic sandstones and conglomerates of the Bradbury formation (Fig. 1a–2). The fluvial rocks of the Bradbury formation contain detrital igneous minerals (sanidine, plagioclase, pyroxene, and olivine) and clasts carried from mafic and trachytic provenances located in an ancient catchment around the northwestern rim of the crater with minor alteration indicated by phyllosilicate formation (Grotzinger et al., 2015; Le Deit et al., 2016; Siebach et al., 2017). Fractional crystallization of alkaline and subalkaline felsic magmas can explain the chemistry of detrital sanidine and plagioclase analyzed within sedimentary rocks and the compositional range of igneous floats observed on the crater floor within the Bradbury formation (Payré et al., 2020; Sautter et al., 2015; Udry et al., 2018).

Lacustrine mudstones of the Murray formation interfinger with the Bradbury formation and are exposed in overlying layers making up the first several hundred meters of Aeolis Mons (Fig. 1a–2; Grotzinger et al., 2015; Stack et al., 2019). The tridymite-containing Buckskin sample was found in the lowermost exposed member of the Murray formation, the Pahrump Hills member, which includes ∼25 vertical m of strata (Fig. 2). Portions of the Murray formation along the rover's traverse are obscured by the Stimson formation, an unconformable eolian sandstone that was deposited above both the Bradbury and Murray formations at a much later time (Banham et al., 2018).

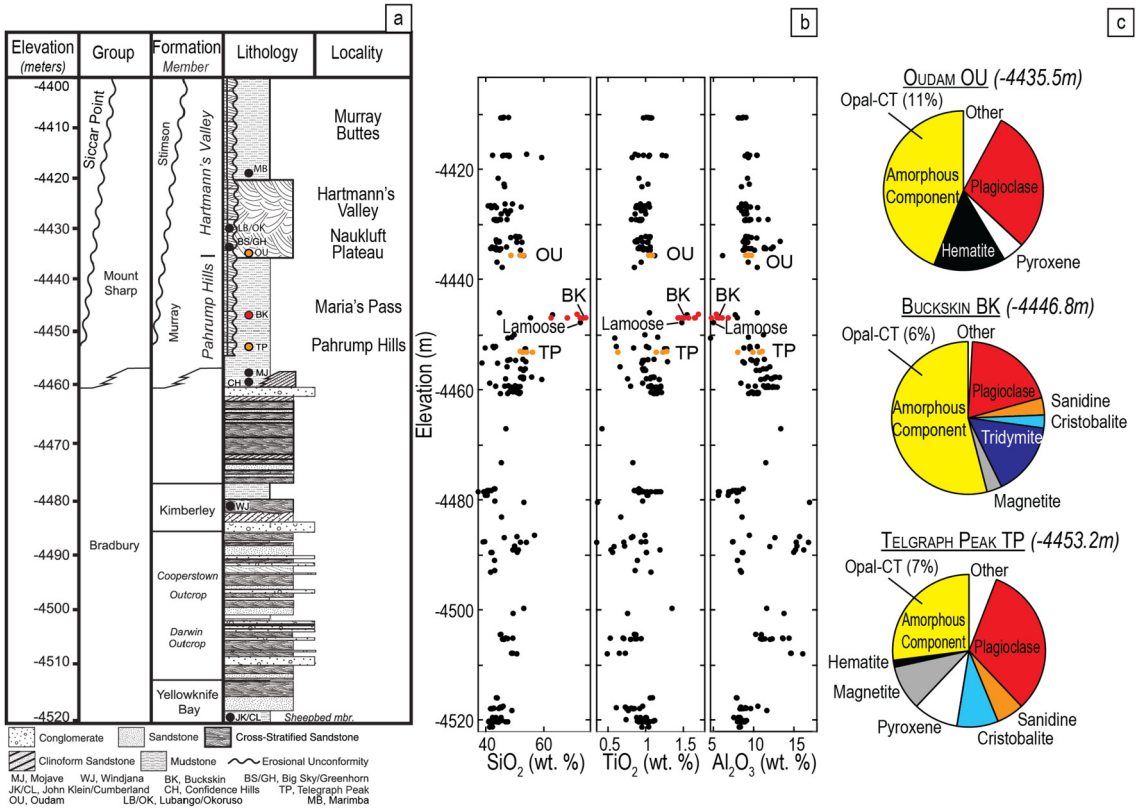


**Fig. 2.** (a) Stratigraphic column of sedimentary units in Gale crater, Mars. Credit: Sedimentology and Stratigraphy working group of the MSL Science Team. (b) $SiO_2$, $TiO_2$, and $Al_2O_3$ concentrations (in wt. %) versus elevation (in m) of sedimentary rocks analyzed by APXS. Buckskin (BK) compositions are in red, and Telegraph Peak (TP) and Oudam (OU) are in orange. Lamoose composition is also indicated for reference. (c) Proportions of mineral phases as measured by CheMin within Telegraph Peak, Buckskin, and Oudam (from the bottom to the top).

The Pahrump Hills member was observed in detail by the rover in two key localities, Pahrump Hills and Marias Pass (Fig. 1a–2). The Pahrump Hills member contains ∼13 m of laminated mudstones and minor cross-stratified sandstones, interpreted to have formed from river-generated hyperpycnal plumes entering a lake (Stack et al., 2019). The sediments are dominated by detrital basaltic igneous minerals, secondary phyllosilicates and iron oxides, and amorphous materials (Rampe et al., 2020). The Telegraph Peak sample (Fig. 2), drilled near the top of the Pahrump Hills locality exposure, contains abundant cristobalite and an X-ray amorphous component with $SiO_2 = 53$ wt.% compared to an average in the Murray formation of 49 wt.% (Fig. 2b; Rampe et al., 2020). From the Pahrump Hills locality, the rover drove ∼500 m across a topographic depression to "Marias Pass" where the rover could access the Murray formation just below the Stimson unconformity.

The Marias Pass locality exposes ∼4-5 meters of Murray strata, with a ∼1 m thick conformable stratigraphic interval of laminated lacustrine strata with high silica content (>70 wt.%; Czarnecki et al., 2020a,b; Frydenvang et al., 2017) near the top of the exposure. No unconformities or visible changes in sedimentation style (such as those that would be expected from subaerial exposure or direct ashfall deposits) were observed throughout Marias Pass in comparison to Pahrump Hills, although the laminations were thinnest (∼0.5 mm thick) in the Si-rich interval, consistent with more distal deposition in a lake (Morris et al., 2016; Hurowitz et al., 2017; Rampe et al., 2017). The Si-rich interval was drilled at the Buckskin target and found to contain monoclinic tridymite and cristobalite as well as significant amorphous silica ($SiO_2 = 75.9$ wt.%; Morris et al., 2016). The tridymite was interpreted to come from silicic volcanism, potentially originating from evolved trachytic rocks in the crater rim or central peak of Gale (Morris et al., 2016).

The final ten vertical meters of the Pahrump Hills member were not analyzed in detail by the rover because they were obscured along the traverse by the overlying Stimson sandstone. The next location above Buckskin with compositional measurements in the Murray formation was in the Hartmann's Valley member, which is a fine-grained cross-stratified sandstone interpreted as eolian reworking of lacustrine sediments (Rampe et al., 2020). The lowest-elevation Oudam target (Fig. 2) drilled from the Hartmann's Valley member has ∼7 wt.% opal-CT and a particularly $SiO_2$-rich X-ray amorphous component relative to other Murray formation samples except for Buckskin (64 wt.% compared to average ∼49 wt.%; Rampe et al., 2020).

The distribution of silica enrichment throughout the Murray stratigraphy is not well constrained, but broadly there is some enrichment in cristobalite ∼5 m below Buckskin, ∼1 m of very high $SiO_2$ at Buckskin, and relatively elevated $SiO_2$ ∼ 10 m above Buckskin. The Telegraph Peak mudstone, located ∼5 meters below Buckskin (Fig. 2a), contains cristobalite (12 wt.%) and plagioclase, but the composition of the amorphous component is dramatically different with 20 wt.% less $SiO_2$ and ∼four times more $FeO_T$ in Telegraph Peak than Buckskin (17.1 wt.% versus 4.8 wt.%; Rampe et al., 2020). Despite the lack of compositional measurements upsection from Buckskin, the Murray rocks immediately above the high-silica layer show elevated but decreasing silica contents based on ChemCam observations (from 75 wt.% $SiO_2$ to ∼52 wt.% $SiO_2$, ; Frydenvang et al., 2017). Ten meters above Buckskin (Fig. 2a), the Oudam's amorphous component contained more $SiO_2$ than most samples analyzed by CheMin in the Murray formation, although ∼10 wt.% less than Buckskin (Table 1; Rampe et al., 2020). Unlike Buckskin, Oudam does not have crystalline silica polymorphs, plagioclase is in higher abundance (52 wt.% versus 43 wt.% in the

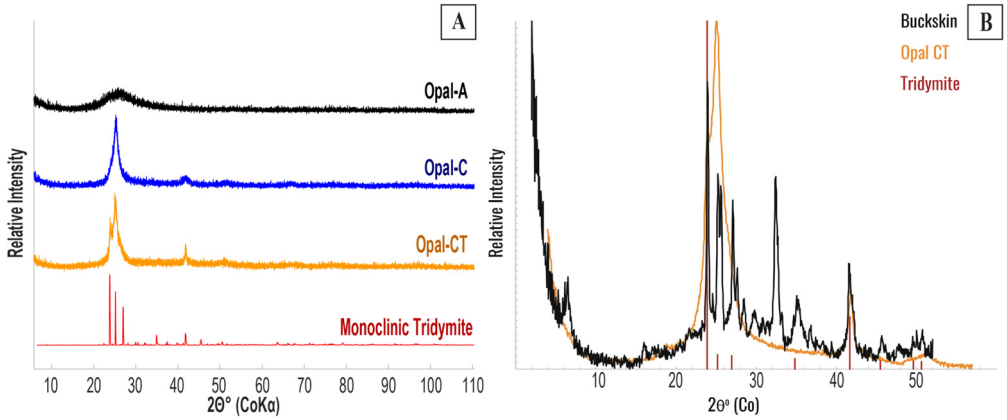


**Fig. 3.** (a) X-ray diffraction patterns of opal-A (black line), opal-C (blue line), opal-CT (orange line), and monoclinic tridymite (red line) from rruff database (https://rruff.info) Degrees-2 theta were converted from a Cu source to a Co source to be consistent with CheMin XRD spectra. (b) X-ray diffraction pattern of the Buckskin mudstone (black) as analyzed by the CheMin instrument. An XRD spectrum of Opal-CT (yellow) and peak locations for monoclinic tridymite (red lines) are shown. (For interpretation of the colors in the figure(s), the reader is referred to the web version of this article.)

crystalline component Rampe et al., 2020), and hematite is abundant.

As of the writing of this manuscript, *Curiosity* has traversed over 380 m of vertical stratigraphy within the Murray formation and has not identified any other locations with either any crystalline tridymite or an X-ray amorphous component as high in silica content as that of Buckskin in Marias Pass.

### 2.2. Composition and mineralogy of Buckskin

The CheMin instrument onboard *Curiosity* measures XRD patterns of scooped eolian sediments and drilled rock powders (grain size sieved to <150 µm; Blake et al., 2012). XRD measurements on the Buckskin mudstone revealed the presence of well-ordered monoclinic tridymite and cristobalite, along with a Si-rich amorphous component likely containing opal-CT and opal-A and/or rhyolitic glass (Fig. 2; Morris et al., 2016). The sample contains a significant Si-rich amorphous component (54 wt.%), plagioclase with an anorthite component $An_{41(3)}$ (19.8 wt.%), and monoclinic tridymite (15.6 wt.%), and minor sanidine with an orthoclase component $Or_{77(14)}$ (3.7 wt.%), magnetite (3.2 wt.%), cristobalite (2.8 wt.%), and anhydrite (0.9 wt.%) (Morrison et al., 2018; Rampe et al., 2020). As emphasized by Morris et al. (2016), the presence of all of the high-intensity diffraction peaks characteristic of monoclinic tridymite reveals the fully-ordered nature of the tridymite in contrast to opaline silica (Fig. 3; detailed in Text S1).

The composition of Buckskin presented in Morris et al. (2016) was measured by APXS (Table 1; Text S2). In contrast to other Pahrump Hills drilled samples, which contain $SiO_2$ concentrations ~48-52 wt.% (Rampe et al., 2020), Morris et al. (2016) show that Buckskin is Si-rich ($SiO_2$ ~ 73.9 wt.%), and depleted in all other major oxides, with only 5.7 wt.% $Al_2O_3$ (Table 1). $TiO_2$, while low by terrestrial standards, is elevated at Buckskin compared to all other samples observed in Gale crater (1.57 wt.%, compared to average 1.0±0.2 wt.%). Buckskin's X-ray amorphous component chemistry is calculated from the CheMin and APXS measurements, as presented by Rampe et al. (2020): the amorphous component chemistry is estimated as the excess elements measured by APXS after subtracting the crystalline component compositions as inferred by CheMin unit-cell parameters. This technique for determining the X-ray amorphous component necessarily relegates minor elements that are not structurally required for observed minerals into the amorphous component, as well as any minerals below the CheMin detection limit of ~2%. These limitations obscure the mineral host of the $TiO_2$, so the $TiO_2$ is partitioned to the amorphous component. Only 1.57 wt.% of a Ti-oxide would account for all of the $TiO_2$. Morris et al. (2016) show that, consistent with the major occurrence of Si-rich materials (opal-CT and opal-A and/or Si-rich glass), Buckskin's X-ray amorphous component is Si-rich ($SiO_2$ = 75.9 wt.%), and depleted in all other oxides, especially $Al_2O_3$ with only 0.04 wt.% $Al_2O_3$ (Table 1).

**Table 1**
Composition of Buckskin as measured by APXS and its crystalline and amorphous component, renormalized to 100 wt.%.

| | APXS[1] | Crystalline[2] | Amorphous[2] |
|---|---|---|---|
| $SiO_2$ | 73.8 | 71.1 | 75.9 |
| $TiO_2$ | 1.57 | 0.00 | 2.81 |
| $Al_2O_3$ | 5.67 | 12.88 | - |
| $Cr_2O_3$ | 0.10 | 0.00 | 0.18 |
| FeOT | 5.50 | 6.40 | 4.80 |
| MnO | 0.09 | - | 0.16 |
| MgO | 0.82 | - | 1.47 |
| CaO | 3.06 | 4.22 | 2.14 |
| $Na_2O$ | 2.08 | 3.27 | 1.15 |
| $K_2O$ | 0.96 | 1.11 | 0.85 |
| $P_2O_5$ | 1.25 | - | 2.24 |
| $SO_3$ | 4.81 | 1.06 | 7.75 |
| Cl | 0.29 | - | 0.52 |

[1] APXS composition in wt.% of post-sieved Buckskin rock from Morris et al. (2016) and Morrison et al. (2018b).
[2] The crystalline and amorphous component compositions in wt.% are from Morrison et al. (2018b).

## 3. Formation of tridymite

### 3.1. Silica polymorphs and metastable states

Silica polymorphs including quartz, tridymite, and cristobalite share a simple formula ($SiO_2$), but their crystal structures differ from each other, imparting distinct physical and chemical properties. Silica polymorphs can form metastable structures at temperatures outside of their stability field. In its typical stability field (870 °C < T < 1470 °C), tridymite is hexagonal, referred to here as high-temperature (T) tridymite, but various metastable low-temperature orthorhombic and monoclinic tridymite structures (< ~420 °C) have been observed in natural and synthetic materials (Deer et al., 2013). These metastable structures form and persist when mineral cooling is rapid and there is insufficient activation energy to break chemical bonds to form a more stable silica polymorph like quartz (Deer et al., 2013; Dollase and Baur, 1976).

**Table 2**
Summary of the characteristics of the tridymite formation pathways as observed in natural settings.

| | Settings | % Tridymite | Minerals of interest | Notes |
|---|---|---|---|---|
| Impact Melt Crystallization | Impact Structure | A few vol.% | - Tridymite<br>- Cristobalite<br>- Feldspar<br>- Magnetite<br>- Glass<br>- Quartz | Crystallization of quartz after tridymite due to relatively slow cooling and/or the presence of impurities |
| Hydrothermal Alteration | →Geothermal fields<br>→Fumaroles | Various amounts | - Tridymite<br>- Cristobalite<br>- Feldspar<br>- Anhydrite<br>- Magnetite<br>- Opal | - Additional secondary minerals expected due to various temperature range<br>- T of fluids mainly below the tridymite stability field |
| Magmatic Crystallization | (Extra-) Terrestrial Volcanic | Up to 44 vol.% | - Tridymite<br>- Cristobalite<br>- Feldspar<br>- Magnetite<br>- Glass | Sometimes quartz when relatively slow cooling and/or impurities in the melt |
| Vapor Crystallization | →Ignimbrite Consolidation | Up to ∼22% | - Tridymite<br>- Cristobalite<br>- Feldspar | Magmatic quartz often associated |
| | →At the vent | Up to 8 wt.% | - Tridymite<br>- Cristobalite<br>- Feldspar | - Minerals in ashes<br>- Minor to no quartz |

All known monoclinic tridymite samples, natural and synthetic, are formed during fast cooling by a series of phase transitions from the stable high-T tridymite (e.g., Dollase and Baur, 1976; Jackson et al., 2011). The sequence of phase transitions for tridymite is still not well constrained, partly because of the influence of initial composition, thermal history, and degree of structural disorders within the initial tridymite (e.g., Pryde and Dove, 1998 and references therein). Roughly, high-T hexagonal tridymite can be reversibly transformed to orthorhombic tridymite at ∼420 °C, which can be reversibly modified to low-T monoclinic tridymite at lower temperatures (<200 °C; Kihara, 1978). All the forms of tridymite are distinct from the disordered structure of opaline silica (Fig. 3a; Eversull and Ferrell, 2008).

### 3.2. Environments where tridymite forms

Natural monoclinic tridymite seems to be extremely rare on Earth and has only been reported in five locations. Four locations correspond to silicic volcanic complexes at Yugawa and Mt Myoho in Japan (Kawai et al., 1978), and in granophyres within the Skaergaard intrusions in Greenland (Larsen and Tegner, 2006). In these settings, tridymite crystallized from a hot silicic magma. Monoclinic tridymite grains have also been identified within impact-melt clasts in the Chesapeake Bay impact crater, Virginia (Jackson et al., 2011). While rare on Earth, monoclinic tridymite is commonly observed in extra-terrestrial samples including lunar basalts and martian meteorites (e.g., Dollase et al., 1971; Mason, 1972; Bridges et al., 1995; Xirouchakis et al., 2002). Synthetic monoclinic tridymite is made as refractory silica bricks, which are fabricated from fired quartz at ∼1400 °C (Schneider et al., 1980), from melting of silica and Na-tungstate at ∼1400 °C (Hoffmann, 1967), or from silica glass under hydrothermal conditions at ∼1100 °C (Nukui and Nakazawa, 1978). In all cases, monoclinic tridymite formed from high-T hexagonal tridymite during fast cooling. Text S3 and Table 2 details terrestrial and extra-terrestrial settings where tridymite has been observed.

### 3.3. Magmatic crystallization modeling

Typically, magmatic tridymite crystallizes from felsic magma, which is rarely observed on Mars (Sautter et al., 2016). Here, we use the MELTS family of thermodynamic models (Ghiorso and Sack, 1995) to explore magmatic conditions that could produce tridymite and other minerals found at Buckskin from martian mantle compositions. Since Buckskin is a sedimentary rock, the igneous minerals present might come from several provenances, but given the abundance of tridymite and lack of mafic minerals in Buckskin, the potential magma that formed tridymite is likely the major contributor. Previous work modeled the formation of felsic rocks including trachytes and diorites found within the Bradbury formation along with detrital igneous minerals originating from evolved magmas (Payré et al., 2020), here we investigate whether the same melts might form tridymite.

Payré et al. (2020) used the crystal chemistry of the detrital igneous minerals of the Bradbury formation to identify a minimum of two magmatic pathways that could have produced the observed igneous minerals. Thermodynamic modeling of igneous-phase equilibria using alphaMELTS software (Smith and Asimow, 2005) showed that detrital sanidine and plagioclase from the Bradbury formation likely formed through fractional crystallization of trachy-andesitic and andesitic to rhyolitic liquids, respectively (Payré et al., 2020). Here, we investigate whether the same magmas would produce tridymite, cristobalite, and feldspar with the compositions observed at Buckskin using the models described in detail in Payré et al. (2020) and Text S4.

We ran fractional crystallization models at 0.2 kbars and oxygen fugacity $fO_2$ fayalite-magnetite-quartz (FMQ) buffer FMQ+1 with $H_2O$=0 and 0.5 wt.% with the rhyolite-MELTS model (Gualda et al., 2012) in the alphaMELTS 2 interface (Antoshechkina and Ghiorso, 2018), which is valid at <10 kbars for mafic and felsic magmas (Text S4). Feldspar, pyroxene, spinel, and tridymite are fractionated from magmas formed by high extent of melting of a mantle source (Fig. 4).

Fractional crystallization forms feldspar with crystal chemistries transitioning from plagioclase to alkali feldspar in late-stage of crystallization (Fig. 4c). Plagioclase composition ranges from $An_{2-70}$, regardless of the initial mantle melt fraction and wa-

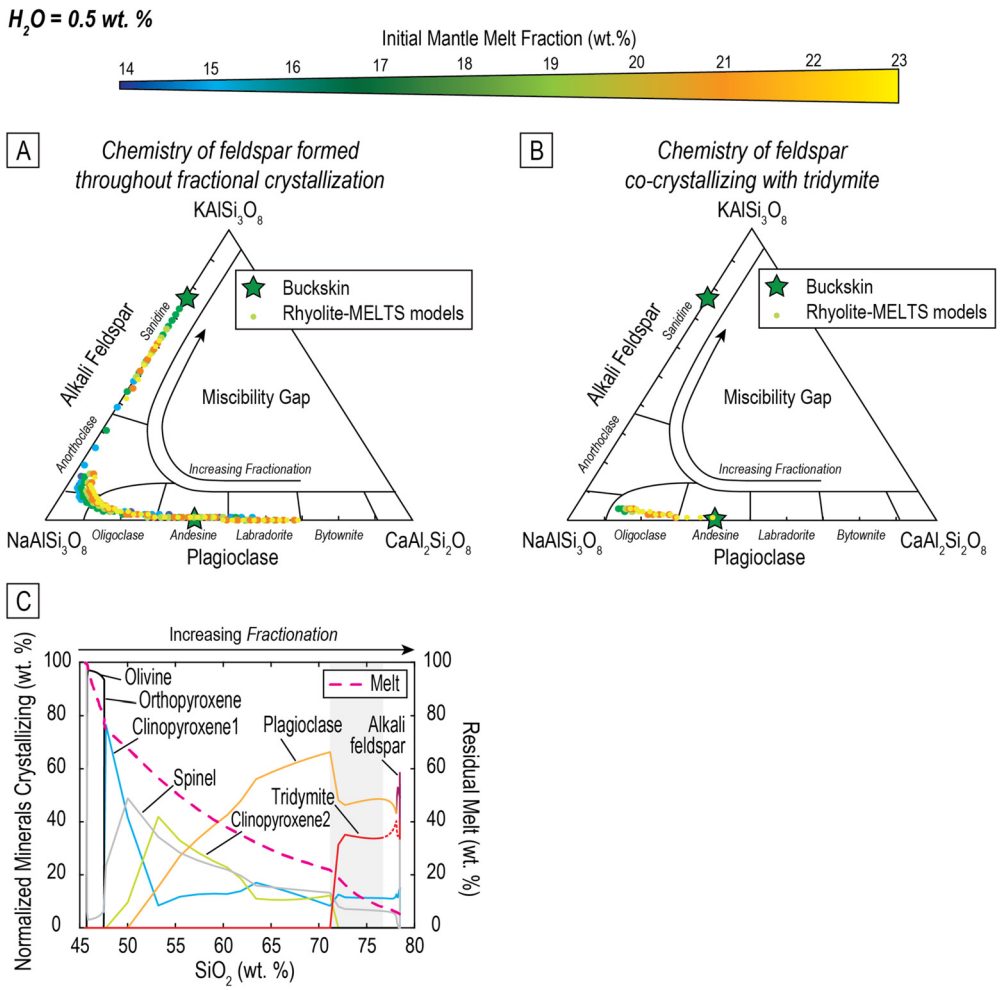


**Fig. 4.** (a) Ternary diagram displaying the crystal chemistry of all feldspar compositions formed during a complete fractional crystallization sequence of magma modeled with rhyolite-MELTS. The models use magma formed by partial melting of a primitive mantle composition (Taylor, 2013) that goes through fractional crystallization with an oxygen fugacity of FMQ +1 at a pressure of 0.2 kbars, and with 0.5 wt. % $H_2O$, selected based on other rocks in Gale crater, modified from Payré et al. (2020), and explained in the text and S4. Color of dots corresponds to the fraction of the mantle composition that melts to form the initial magma that goes through fractional crystallization. The compositions of the two feldspars measured in Buckskin by CheMin XRD are shown as green stars. (b) Ternary diagram of the subset of feldspar compositions that crystallize simultaneously with tridymite during fractional crystallization of the same magma. (c) $SiO_2$ concentration of the residual liquid versus the abundances of minerals (in wt.%; normalized to 100 wt.% crystalline) crystallizing during fractional crystallization of the same magma formed with 23 wt.% mantle melt (yellow dots above). The amount of melt remaining (wt. %) is shown with a dashed pink line; overall, $SiO_2$ concentrations of the residual liquid increase with the degree of fractionation. The range of $SiO_2$ values while tridymite crystallizes with plagioclase is indicated with a light gray box. For example, a liquid with $SiO_2$ ~ 72 wt.% crystallizes various phases including ~38 wt.% of tridymite and ~45 wt.% of plagioclase. The dashed red line corresponds to a non-tridymite silica polymorph crystallizing at T < 870 °C. Lines corresponding to the plagioclase and alkali feldspar components in the alphaMELTS output were merged for clarity (they form a continuum but are labeled distinctly in model output).

ter content (Fig. 4a; Fig S1). Tridymite forms from late-stage rhyolitic magmas produced by fractional crystallization of magmas extracted at ≥15 wt.% of mantle melting. In one model, the tridymite simultaneously crystallized with a plagioclase composition matching Buckskin's ($An_{12-39}$ and $An_{41(3)}$, respectively; 1 $\sigma$ uncertainty from Morrison et al. (2018); Fig. 4b). These two minerals simultaneously crystallize, with up to 48.0 wt.% of plagioclase and 35.1 wt.% of tridymite, when 78 wt.% of a hydrous melt formed by 23 wt.% mantle melting has crystallized (Fig. 4c; Fig. S2).

The Buckskin sample also contained sanidine, an alkali feldspar. Alkali feldspar $Or_{0-73}$ is favored during fractional crystallization of hydrous magmas with low-melting degrees (≤ 17 wt.%) (Fig. 4a; Fig. S1). Although tridymite does not crystallize simultaneously with alkali feldspar, alkali feldspar could have crystallized in the same volcanic system that formed tridymite and plagioclase, the two latter being produced from a higher-initial-melt-degree hydrous magma (here 23 wt.%) than alkali feldspar's (here ≤ 17 wt.%). Higher $fO_2$ values would favor the crystallization of tridymite, plagioclase, and alkali feldspar with compositions matching those of Buckskin's feldspars from a single magma (Fig. S3).

According to the rhyolite-MELTS models, cristobalite never crystallizes. As discussed in Text S4, the absence of cristobalite could be due to the limited experiments producing cristobalite within the database used for calibrating rhyolite-MELTS (Gualda et al., 2012; Hirschmann et al., 2008). Hence, cristobalite might crystallize along with feldspar and tridymite from late-stage melts (Fig. 4), form from a high-T Si-rich magma recharged in the chamber, or be a vapor-phase.

## 4. Formation pathways for monoclinic tridymite at Buckskin

In this section, we review known and hypothesized formation mechanisms for tridymite to suggest the most plausible way(s) to form the monoclinic tridymite identified in the Buckskin sample. In order to be validated, the formation model must explain:

(1) The amount and form of tridymite (15.6 wt.% monoclinic tridymite);

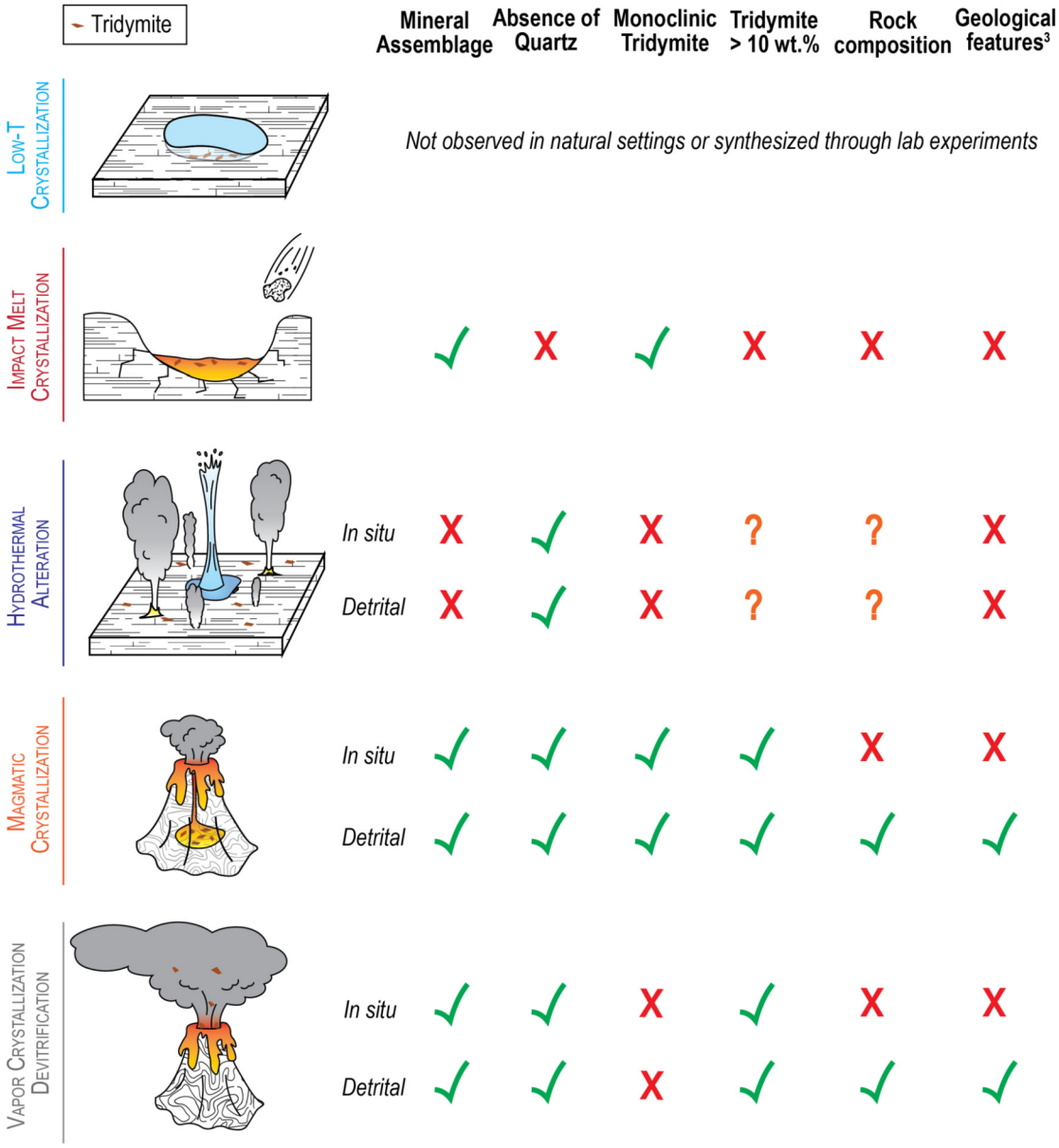


**Fig. 5.** Summary of major pros and cons for each envisioned scenario for the formation of the Buckskin sample. A box is checked when observations in the associated natural setting are consistent with Buckskin's characteristics. 'X' means that observations in the associated natural setting do not match characteristics of Buckskin. '?' represents uncertainty: the literature describing the associated natural setting do not describe the criterion or do not describe it with enough detail to know whether it is consistent with Buckskin.

(2) the mineral assemblage of the Buckskin sample including plagioclase (19.8 wt.%), tridymite (15.6 wt.%), minor sanidine (3.7 wt.%), cristobalite (2.8 wt.%), and a significant Si-rich X-ray amorphous component (54 wt.%), magnetite (3.2 wt.%) and anhydrite (0.9 wt.%);

(3) the absence of quartz within the Buckskin sample and surrounding samples;

(4) the composition of the Buckskin mudstone, particularly the low amounts of $Al_2O_3$ (5.67 wt.%) and other non-$SiO_2$ oxides except $TiO_2$; and

(5) the geological context of the sample as a conformable laminated lacustrine mudstone.

The following subsections and Fig. 5 describe pros and cons of each formation mechanism that could have led to the formation of monoclinic tridymite. A detrital origin is preferred based on: (1) geological context of Gale crater being a paleo-lake fed by streams and groundwater (Stack et al., 2019), (2) low-T mineralogy within the Murray formation, (3) preserved conformable thin laminae (0.5 mm) consistent with lacustrine deposition, without unconformity or change of sedimentation style that is expected from a lava flow or direct ashfall in Buckskin, and (4) low $Al_2O_3$ concentration of Buckskin amorphous component inconsistent with Si-rich glass.

### 4.1. Low-temperature processes

While the geologic context of the Buckskin sample is consistent with authigenic precipitation of silica, low-T precipitation of any form of crystalline tridymite outside of its stability field has never been observed in natural samples or synthesized in the lab. The Buckskin XRD pattern displays clear monoclinic tridymite peaks distinct from opaline silica (Fig. 3a; Eversull and Ferrell, 2008). The only known way to form natural or synthetic monoclinic tridymite is through the formation of high-T tridymite. Without any further lab experiments, low-T precipitation of monoclinic tridymite is unlikely (Fig. 5).

**Table 3**
Mineralogical assemblages including tridymite detected within a few hydrothermal settings on Earth.

| Locations | Mineral Assemblages | | | References |
|---|---|---|---|---|
| | *Temperature Decreasing* | | | |
| Mount Augustine, USA | Tridymite, anhydrite | Tridymite, hematite, Fe-oxide, Fe- chloride, metallic phases | Anhydrite, halite, sylvite, tridymite | (Getahun et al., 1996) |
| Kudryavy, Russia | Tridymite, albite, sanidine, garnet, Fe- and Al- oxides, and cristobalite | Tridymite, cristobalite, anhydrite, Al- and Fe-sulfates, and Ti-oxides | | (Ganino et al., 2019) |
| Humazo Field, Argentina | Smectites, kaolinites, zeolites, tridymite, cristobalite, and quartz | | | (Mas et al., 2000) |
| Mount Rainier, USA | Illite, pyrite, quartz, tridymite | Kaolinite, opal/tridymite, pyrite ± alunite | Smectite, halloysite, kaolinite, cristobalite, tridymite, opal, alunite, gibbsite, and calcite | (John et al., 2008) |

### 4.2. Impact melt crystallization

Tridymite is a small proportion of the rock (0.3-5 vol.%) in the terrestrial Popigay impact crater and is found in a 5 cm interval within the core drilled in the Chesapeake Bay impact structure (Text S3; Table 2). However, these amounts are low compared to the quantity of tridymite within the Buckskin sample (15.6 wt.%), so it would be difficult to explain the high concentration of tridymite at Buckskin from an *in-situ* impact melt or an impact melt from which detritus was sourced (Fig. 5). Furthermore, the transformation of tridymite and/or cristobalite to quartz is systematically observed in terrestrial impact structures (Text S3), which contrasts with the absence of quartz in Buckskin. Finally, the absence of an impact crater in the vicinity of Buckskin and the fine-scale laminated nature of the Murray formation are inconsistent with an *in-situ* impact melt. Although impact craters are common within and around Gale crater, the sedimentary record would likely preserve other impact signatures. The impact melt scenario is thus not favored.

### 4.3. Hydrothermal alteration

A hydrothermal formation process for Buckskin tridymite has been suggested by Yen et al. (2021) in which *in-situ* warm fluids circulate at the surface or just underground and reach temperatures high enough to form tridymite (>870 °C). However, high-T alteration of primary minerals like feldspar present throughout the Murray formation would lead to a wide range of minerals including zeolites, phyllosilicates, and/or oxides as observed in Kudryavy volcano, Russia (Africano et al., 2003) and Mount Rainier, USA (Table 3; Text S3; John et al., 2008) The diverse mineralogical assemblages expected from fluid temperature zoning have not been observed in Gale crater (Fig. 5). Instead, the Murray formation mostly contains basaltic mineral detritus and low-T minerals including smectite, and does not present significant mineralogical variability except for the Buckskin layer itself (Achilles et al., 2020; Rampe et al., 2020). Geochemical variations are relatively minor and can be explained by redox stratifications (Hurowitz et al., 2017) and/or groundwater diagenesis (Rampe et al., 2020) without any need for elevated temperatures. Furthermore, temperatures from burial diagenesis in the crater are not expected to have exceeded 125 °C (Borlina et al., 2015).

Texturally, no features characteristic of fumarolic activity or hydrothermal alteration, like the opaline silica nodules from Gusev crater, Mars (Ruff and Farmer, 2016), colored layers/patches (e.g., Getahun et al., 1996), or vents as observed within the fumarolic field of the Kydruavy volcano (Africano et al., 2003; Ganino et al., 2019), are identified within the Buckskin mudstone vicinity. At a larger scale, rover and orbital imaging did not detect any volcanic structures in Gale crater (e.g., Malin, 2000; Milliken et al., 2010). $SiO_2$-rich light-toned fracture-associated halos were found around the contact between the Murray and overlying Stimson. If those was a conduit for hydrothermal fluid circulation, temperatures might be expected to be at their highest values in the fractures, but they do not contain high-T phases and are instead dominated by opal-A (Yen et al., 2021). The consistent thinly laminated fine-grained bedrock of the Murray formation (Grotzinger et al., 2015; Stack et al., 2019), with detrital igneous minerals and low-temperature secondary mineral assemblages (Hurowitz et al., 2017; Rampe et al., 2020), is more consistent with lacustrine deposition. Relationships with other potential hydrothermal signatures in Gale are discussed in Text S5.

### 4.4. Magmatic crystallization

Under low-pressure conditions, rhyolitic magmas can produce significant amounts of tridymite during cooling and crystallization (Fig. 5). Some extra-terrestrial samples contain up to 44 vol.% tridymite (Text S3; Table 2; Bischoff et al., 1993). On Earth, quartz commonly accompanies or replaces tridymite in natural samples, likely due to slow cooling (Dollase and Baur, 1976), or impurities like Na that could favor the transformation of tridymite to quartz (details in Text S3). The absence of quartz within Buckskin and other CheMin samples in the vicinity (Rampe et al., 2020) suggests rapid cooling of the magma.

Based on rhyolite-MELTS models, tridymite and plagioclase in Buckskin could be late-stage products of the evolution of the same magmatic source that formed the plagioclase grains found in the Bradbury formation (orange/yellow dots in Fig. 4a-b). Under specific conditions (0.5 wt % water, ≥21 wt.% partial melting; Payré et al., 2020), up to 53.4 wt% plagioclase and up to 35.1 wt.% tridymite crystallize from 21.8 wt.% residual melt. Crystallization of the sanidine observed at Buckskin requires a lower

degree of melting or different $fO_2$ conditions (Fig. S3). Therefore, sanidine and plagioclase/tridymite either come from a different source, a different eruption from the same source, or all may have erupted together after settling for some settling time in the magma plumbing system. Spinel and augite crystallize simultaneously with plagioclase and tridymite but are not observed within Buckskin (Fig. 4c; Fig. S1). This discrepancy can be explained by the sinking of these dense minerals at the bottom of the magmatic system, while lighter, floating, feldspar and tridymite erupted. The unknown $TiO_2$-bearing phase could correspond to either minor spinel, if incorporated below detection limits (∼2 wt.%), and/or Si-rich glass. According to Kushiro (1975), $Ti^{4+}$ and $P^{5+}$ are polyvalent cations that favor the crystallization of polymerized minerals including tridymite and cristobalite in magmas, resulting in P-Ti-rich melts crystallizing abundant silica minerals compared to P-Ti-depleted melts. This is in agreement with the elevated $TiO_2$ and $P_2O_5$ concentrations in Buckskin amorphous component.

Based on the models, magmas are rhyolitic when tridymite crystallizes with $SiO_2 = 73 - 80$ wt.% (Fig. S4), similar to that of the Buckskin amorphous component, which is a mixture of opaline silica and rhyolitic glass. However, modeled alkali and $Al_2O_3$ contents would be higher in a rhyolitic glass than observed in the amorphous component (Fig. 6; Table 1). The Buckskin amorphous component has ∼0 wt.% $Al_2O_3$ but natural rhyolitic glasses from nearly all recorded terrestrial igneous rocks have $Al_2O_3 > 5$ wt.% (Fig. 6). Buckskin's composition is not consistent with direct sampling of a volcanic magma or ashfall, but can be explained by a detrital origin as suggested by Morris et al. (2016). Grain-size and density differences between minerals would affect their transport distance into the lake, changing the ratios between detrital minerals and potentially further enriching tridymite or leaving denser mafic minerals closer to shore. The dissolution of rhyolitic glass would create silica-saturated lakewater that would precipitate Si-rich products including opaline silica, which would dilute the oxide contents in the sediments. Dissolution of rhyolitic glass would also induce precipitation of Al-bearing secondary minerals; in an analogous terrestrial lake deposit, the Al minerals are observed in patchy zones within the Tecocomulco Lake sediments, Mexico (Roy et al., 2009b).

For all the reasons stated above, a detrital origin is consistent with Gale crater geological context, lack of volcanic features in Gale crater (Malin, 2000; Milliken et al., 2010), and Buckskin's texture and composition.

### 4.5. Vapor crystallization and devitrification

Vapor-phase crystallization, which is the growth of crystals from hot gas streams within pore spaces, can occur at a volcanic vent during an eruption, when minerals precipitate from hot vapor. Devitrification is the crystallization of glass after emplacement of ashes. Tridymite can be a major $SiO_2$ phase formed from vapor crystallization since forming at high temperatures and low pressures; at the Soufriere Hills Volcano (SHV), Montserrat, up to 8 wt.% vapor tridymite crystallized and was associated with little or no quartz in addition to plagioclase and alkali feldspar (Baxter et al., 1999). Such amount of tridymite is not sufficient to match CheMin observations in Buckskin and other processes are needed such as devitrification, which can produce up to 22 wt.% of tridymite in addition to feldspar, cristobalite, and Fe-Ti-oxides as observed in the rhyolitic Grey's Landing ignimbrites (Heled et al., 2022). Vapor crystallization of a Ti-oxide such as ilmenite has been observed in vugs in lunar basalts (McKay et al., 1972). An explosive eruption could thus explain the phases observed at Buckskin including tridymite, cristobalite, feldspar, Ti-oxide, and rhyolitic glass.

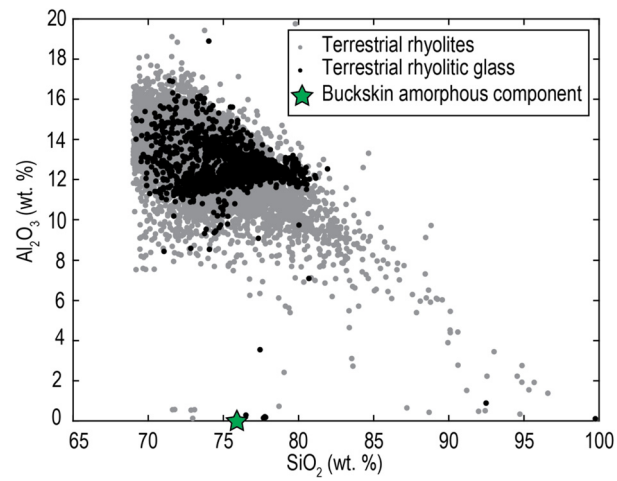


**Fig. 6.** $Al_2O_3$ versus $SiO_2$ contents of all terrestrial rhyolites (gray dots; http://georoc.mpch-mainz.gwdg.de/georoc/) and rhyolitic glass (black dots; http://georoc.mpch-mainz.gwdg.de/georoc/) reported in GEOROC, compared to the Buckskin amorphous component as measured by CheMin and APXS (green star; Rampe et al., 2020). Extremely low bulk $Al_2O_3$ concentrations are rare; only four volcanic provinces on Earth with $SiO_2$ contents between 70 and 80 wt.% erupted rhyolites with bulk $Al_2O_3$ concentrations close to the Buckskin amorphous component (Iberian Peninsula, Portugal; Taupo volcanic zone, New Zealand; Svecornowigian Province and Kola-Lapland Province, Baltic shield), and Taupo volcanic zone. All Al-depleted glass contains $TiO_2 > 12$ wt.%, i.e., well above the Buckskin $TiO_2$ concentration of 1.57 wt%. The composition of the Buckskin amorphous component is not consistent with any terrestrial rhyolitic glass reported in GEOROC. Note that Mars crust and Earth continental and oceanic crust present similar $TiO_2$ concentrations (0.98 wt.% versus 0.6 – 1.1 wt.%; Rudnick, 2018; Taylor and McLennan, 2009; White and Klein, 2014), which thus cannot explain the significant difference in $TiO_2$ concentrations between the terrestrial Al-depleted rhyolitic glass and Buckskin.

As discussed in Section 4, the direct deposition of ashes containing rhyolitic glass would result in an amorphous composition closer to that of natural rhyolitic glasses (Fig. 6) and would create an unconformity and a change in bedding style with a massive airfall layer, which was not observed (Morris et al., 2016). The deposition of ashes into the lake and watershed and subsequent transport and dilution of those materials, including by precipitation of opaline silica (Smith, 1998), could explain a depletion of other oxides, the presence of opaline silica in the amorphous component, and the thin laminae observed at Buckskin.

## 5. Proposed model for Buckskin formation

The mineralogical assemblage sampled at Buckskin, specifically the 15.6 wt.% tridymite, high abundance of Si-polymorphs, and the absence of any mafic minerals like pyroxene, support a silicic source. The absence of quartz suggests that high-T tridymite crystallized from a magma or hot vapor phase and was rapidly cooled to a metastable monoclinic form (Fig. 5). Direct sampling of an ashfall or igneous deposit is inconsistent with the composition and geologic context of an extremely Al-depleted mudstone with conformable thin laminations (0.5 mm) in lacustrine sediments, so the tridymite is interpreted as detrital. The Si-rich, Al-depleted amorphous component and the uninterrupted fine laminations imply secondary addition of $SiO_2$-rich precipitates in the lacustrine environment. Here, we describe the details of a proposed formation scenario for the Buckskin mudstone.

### 5.1. Constraints on timing of tridymite deposition

The stratigraphic context of Buckskin constrains the relative timing of the felsic eruption. If tridymite-containing rocks were eroded to form an exposed outcrop within the Murray watershed (crater rim or central peak), as suggested by Morris et al. (2016),

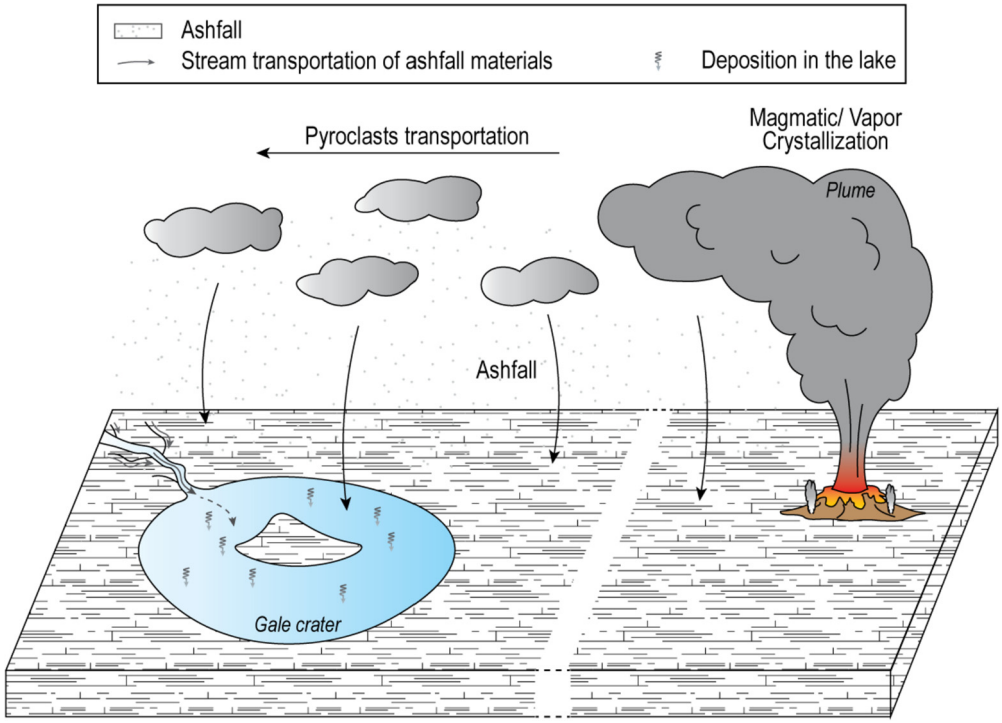


**Fig. 7.** Sketch of our preferred formation and deposition pathway of tridymite in the Buckskin sample. The location of the volcano is currently unknown but could be several to thousands of kilometers away from Gale crater.

a low, steady trickle or episodic pulses of tridymite would have been observed throughout the laminated Murray mudstone (e.g., Romans et al., 2016). This is not observed. Instead, the abrupt change in mineralogy compared to the Murray sedimentary rocks sampled below and in hundreds of meters above the Buckskin mudstone suggests a limited supply of silica polymorphs, which cannot be explained by a continuous erosion of tridymite-bearing felsic rocks. The decreasing $SiO_2$ upsection (Fig. 2) broadly suggests a limited supply of $SiO_2$-rich materials, although the ~7 wt.% opal-CT in Oudam, lacking from samples at higher elevations (Rampe et al., 2020), allows for some dispersion of $SiO_2$-rich materials in the stratigraphy. This is more consistent with an influx of tridymite and silicic materials around the time of Buckskin deposition than with exposure of a distinctive rock in the watershed.

### 5.2. Proposed scenario for tridymite deposition

Given these constraints on Buckskin's origin, we propose that a silicic ash-fall deposit containing tridymite, cristobalite, feldspar, Ti-oxide, and Si-glass settled into the lake and watershed of Gale crater during the Hesperian while the Murray formation was being deposited (Fig. 7). Erosion of a loose ash deposit would provide limited supplies of high-silica material for the streams to transport into the lake, thereby limiting the thickness of the resulting high-silica strata. Light fine-grained silicic minerals would be concentrated during transport to the distal portions of the lake, where they deposited as thin layers, suggesting that the percent of erupted tridymite was likely lower than the percent measured in Buckskin. Ashes of rhyolitic glass would be easily dissolved, and some tridymite and cristobalite would dissolve due to their instability in water compared to quartz (Dove and Rlmstidt, 1994; Robie et al., 1978), leading to the formation of a significant amount of Si-rich amorphous material including opal-CT and potential opal-A (Morris et al., 2016). The subsequent precipitation of amorphous $SiO_2$ within the lake water or just below the water-sediment interface likely diluted the oxide concentrations of the overall amorphous component except for the enhancement of $SiO_2$ content. The large amount of tridymite (35.1 wt.%) and plagioclase (48.0 wt.%) crystallizing from a notable amount of hydrous magma coming from 23 wt.% mantle melting (Fig. 4c) agrees with the elevated abundances of tridymite and plagioclase in Buckskin, 34 wt.% and 43 wt.% of the crystalline component, respectively. The elevated $TiO_2$ contents in Buckskin compared to the surroundings (Fig. 2b) is consistent with tridymite-forming magmas (Kushiro, 1975), and is likely due to the occurrence of Ti-rich glass and/or vapor Ti-oxides, as discussed in Section 4. As observed in other drilling sites in Gale crater (e.g., Vaniman et al., 2014), anhydrite in Buckskin likely precipitated in fractures following the lithification of the mudstone. Magnetite could be either a magmatic or a sedimentary product, as suggested by Morris et al. (2016), and could include minor $TiO_2$. The influence of the $SiO_2$-rich ash would have gradually decreased upsection as the ash eroded, with the silica polymorphs decreasing faster due to their instability, consistent with the opal-CT in Oudam and the decreasing $SiO_2$ in Hartmann's Valley.

Key challenges to explaining the Buckskin sample are (1) the lack of any observed change in lake sedimentation style, indicating that direct ashfall deposit into the lake was not observed by the rover, and (2) the compositional and textural requirement that Buckskin is not a direct ash deposit, so the mineral components must be detrital but dominantly silicic. Despite the lack of visual confirmation of an ashfall from the rover, an ashfall is more consistent with the relative purity and distribution of silicic minerals within the stratigraphy than exposure of silicic rocks within the provenance. A sudden influx of ash can dominate the fine-grained transported component in a fluvial-lacustrine system (Roy et al., 2009a,b). Even so, some catchment sediments could have been transported into the crater along with tridymite-bearing ashes, perhaps in volumes too small to be detected with CheMin (<2 wt.%). Pyroxene comprises 9.5 wt.% of Telegraph Peak, so a similar fine-grained component could make up ~10% of the sample at Buckskin without being detected. The decrease of $SiO_2$ and the increase of other oxide concentrations within a meter above Buckskin (Frydenvang et al., 2017) support a relatively rapid increase

in mixing between airfall and catchment materials. Similar mixing phenomena are also observed in Lake Tecocomulco, Mexico (Roy et al., 2009b).

*5.2.1. Terrestrial analog for the proposed scenario*

The dacitic–rhyolitic tephra deposit within Lake Tecocomulco, Mexico, is a good analog for the deposition of pyroclasts within Gale lake (Roy et al., 2009b). Explosive eruptions deposited abundant tridymite, cristobalite, and plagioclase within the Tecocomulco lake and catchment, forming a 255-cm thick lacustrine sedimentary sequence (Roy et al., 2009b). Although the catchment contains mafic rocks (basalt/andesite), no mafic mineral like olivine and pyroxene were observed within the cored lacustrine sediments. Tridymite and cristobalite are identified in amounts up to >30 wt.% in several drill core samples within the lake sediments. Quartz and amphibole are identified in a few samples but are not always present (e.g., dacitic-rhyolitic air-fall tephra layer and silty-sandstones with 10-20 wt.% quartz and >30 wt.% of tridymite and cristobalite, respectively; Roy et al., 2009a,b). Al-bearing halloysite precipitated in a few units within the sequence as a result of intense chemical weathering during the deposition of sediments, but again is not present in all samples (Roy et al., 2009a,b). Unlike the Tecocomulco sedimentary formation, no obvious airfall pyroclastic layers interstratified with the sedimentary sequence such as a coherent bedding were observed in Gale crater. Either such a layer is hidden and not observable along the rover traverse, or the pyroclastic material comes from the watershed only.

*5.2.2. Volcanic source for the proposed scenario*

Tridymite, cristobalite, and feldspar can form from magmatic crystallization within a rhyolitic liquid and/or through vapor crystallization/devitrification. An explosive eruption would have thrown Si-rich ash into the air to land in the Gale crater watershed and perhaps lake, depositing a tridymite-rich layer at Buckskin. The volcanic origin of the tridymite layer cannot be located, especially due to the lack of data to calculate the ash volume deposited in Gale crater and the surroundings. An explosive eruption on Mars from a stratovolcano or a caldera that then collapsed (Michalski and Bleacher, 2013) would generate hundreds-to-thousands $km^3$ of materials, with an ash plume that can travel tens-to-thousands of km away from the volcano depending on various physical parameters such as the surrounding topography, enabling pyroclasts to be widespread. Apollinaris patera is a volcanic edifice located ∼2,100 km away from Gale crater that was active in Early to Mid-Hesperian time and shows evidence of explosive eruptions composed of pyroclastic flows. It has been suggested to be the source of airfall depositions at the Medusae Fossae Formation (MFF), which might be related to the low thermal inertia sediments on the uppermost central peak of Gale. According to Kerber et al. (2013) and considering a significant eruption volume matching MFF volume, ash dispersal models of eruptions at Apollinaris would produce an ash plume that could cause 6.25 m to several hundreds of meters of ashes to be deposited in Gale crater depending on the atmospheric pressure. Although the eruption duration and the density of silica-polymorph and feldspar ash particles could vary from the models, deposition of pyroclastic airfall from a large explosive eruption occurring thousands of kilometers away from Gale is plausible, and could be amplified by eolian transportation from an ashfall to Gale watershed.

A closer volcanic source can be also envisioned. Calderas that collapsed, which can be confused with degraded impact craters as suggested in Arabia Terra, can erupt thousands $km^3$ of materials (Michalski and Bleacher, 2013) and could thus be the origin of the silicic layer in Buckskin. Despite the transparency of Si-polymorphs with infrared spectroscopy, thermal infrared and visible-near infrared observations can detect hydrated silica (e.g., Michalski et al., 2003), which was observed in the vicinity of Gale crater including within a delta in Garu crater located ∼200 km east of Gale (Hauber et al., 2013). Hydrated silica can be formed through various processes (e.g., diagenetic), but the dissolution and transportation of Si-polymorphs and feldspar ashes from the watershed to the delta might explain these unexpected concentrations of hydrated silica. If such a scenario occurred, silicic explosive eruptions on Mars might be overlooked, especially due to the transparency of Si-rich igneous minerals with visible-near infrared spectroscopy.

*5.3. Implications*

Overall, our proposed model is in agreement with a silicic provenance and a detrital origin of tridymite as suggested by Morris et al. (2016) and Czarnecki et al., 2020a,b. A thorough review of natural settings and thermodynamic models suggests magmatic and/or vapor crystallization/devitrification forming tridymite, cristobalite, feldspar, and Ti-oxide. Sedimentary observations argue against *in-situ* volcanics or hydrothermal alteration including fumaroles, and favor contemporaneous ashes falling into Gale crater lake and/or watershed, enhanced by the precipitation of opaline silica. Based on observations in Gale crater, there was at least one instance of explosive silicic volcanism on Mars during the Hesperian. Such explosive volcanism in the Hesperian provides both compositional and timing constraints revealing that Mars magmatism was not restricted to mafic eruptions and crystallization of mafic minerals as suggested by Baratoux et al. (2013). Felsic magmas, potentially similar to intraplate melts on Earth like Icelandic melts (Udry et al., 2018), have formed on Mars from the Noachian (e.g., Sautter et al., 2015) to the Hesperian, and perhaps later on. Ongoing and future missions should seek evidence for additional evolved volcanism and additional constraints on the timing of volcanic eruptions; Mars is not only a basaltic world.

## CRediT authorship contribution statement

**V. Payre**: Conceptualization, Methodology, Software, Investigation, Resources, Writing, Visualization. **K.L. Siebach**: Methodology, Supervision, Funding Acquisition, Writing. **M.T. Thorpe**: Resources, Methodology. **P. Antoshechkina**: Programming, Validation.: **E.B. Rampe**: Resources.

## Declaration of competing interest

The authors declare that they have no known competing financial interests or personal relationships that could have appeared to influence the work reported in this paper.

## Data availability statement

Data associated with this article can be accessed in published papers and are available in Tables 1–3.

## Acknowledgements

We are thankful for the productive and fruitful discussions with Dr. J. P. Grotzinger and J. A. Hurowitz. We are grateful for the thorough reviews from the two anonymous reviewers and the editor Dr. W. B. McKinnon. V.P. was funded by the Wiess/Pan fellowship at the department of Earth, Environmental, and Planetary Sciences at Rice University and the Mars Science Laboratory Participating Scientist program from Dr. M. R. Salvatore (Program solicitation NNH15ZDA001N-MSLPSP, grant number: 15-MSLPSP15_2-0051) and Dr. C. S. Edwards (Program solicitations NNH15ZDA001N-MSLPSP and NNH21ZDA001N-MSLPSP, grant numbers: 15-MSLPSP15_0015 and 80NSSC22K0732, respectively).

P.A. acknowledges funding for the development of alphaMELTS 2 through a NSF grant EAR-1947616. We are also grateful to NASA for providing the following grants: 15-MSLPSP15_2-0051, 15-MSLPSP15-0015, and 80NSSC22K0732.

## Appendix A. Supplementary material

Supplementary material related to this article can be found online at https://doi.org/10.1016/j.epsl.2022.117694.

## References

Achilles, C.N., Rampe, E.B., Downs, R.T., Bristow, T.F., Ming, D.W., Morris, R.V., Vaniman, D.T., Blake, D.F., Yen, A.S., McAdam, A.C., Sutter, B., Fedo, C.M., Gwizd, S., Thompson, L.M., Gellert, R., Morrison, S.M., Treiman, A.H., Crisp, J.A., Gabriel, T.S.J., Chipera, S.J., Hazen, R.M., Craig, P.I., Thorpe, M.T., Marais, D.J.D., Grotzinger, J.P., Tu, V.M., Castle, N., Downs, G.W., Peretyazhko, T.S., Walroth, R.C., Sarrazin, P., Morookian, J.M., 2020. Evidence for multiple diagenetic episodes in ancient fluvial-lacustrine sedimentary rocks in Gale crater, Mars. J. Geophys. Res., Planets 125, e2019JE006295. https://doi.org/10.1029/2019JE006295.

Africano, F., Bernard, A., Korzhinsky, M., 2003. High temperature volcanic gas geochemistry (major and minor elements) at Kudryavy volcano, Iturup Island, Kuril Arc, Russia. Vulcânica 1, 87–94.

Antoshechkina, P.M., Ghiorso, M.S., 2018. MELTS for MATLAB: a new educational and research tool for computational thermodynamics. AGU Fall Meet. Abstr. 44.

Banham, S.G., Gupta, S., Rubin, D.M., Watkins, J.A., Sumner, D.Y., Edgett, K.S., Grotzinger, J.P., Lewis, K.W., Edgar, L.A., Stack-Morgan, K.M., Barnes, R., Bell, J.F., Day, M.D., Ewing, R.C., Lapotre, M.G.A., Stein, N.T., Rivera-Hernandez, F., Vasavada, A.R., 2018. Ancient Martian aeolian processes and palaeomorphology reconstructed from the Stimson formation on the lower slope of Aeolis Mons, Gale crater, Mars. Sedimentology 65, 993–1042. https://doi.org/10.1111/sed.12469.

Baratoux, D., Toplis, M.J., Monnereau, M., Sautter, V., 2013. The petrological expression of early Mars volcanism. J. Geophys. Res., Planets 118, 59–64. https://doi.org/10.1029/2012JE004234.

Baxter, P.J., Bonadonna, C., Dupree, R., Hards, V.L., Kohn, S.C., Murphy, M.D., Nichols, A., Nicholson, R.A., Norton, G., Searl, A., Sparks, R.S.J., Vickers, B.P., 1999. Cristobalite in volcanic ash of the Soufriere Hills volcano, Montserrat, British West Indies. Science 283, 1142–1145. https://doi.org/10.1126/science.283.5405.1142.

Bischoff, A., Geiger, T., Palme, H., Spettel, B., Schultz, L., Scherer, P., Schlüter, J., Lkhamsuren, J., 1993. Mineralogy, chemistry, and noble gas contents of Adzhi-Bogdo– an LL3–6 chondritic breccia with L-chondritic and granitoidal clasts. Meteoritics 28, 570–578. https://doi.org/10.1111/j.1945-5100.1993.tb00280.x.

Blake, D., Vaniman, D., Achilles, C., Anderson, R., Bish, D., Bristow, T., Chen, C., Chipera, S., Crisp, J., Des Marais, D., Downs, R.T., Farmer, J., Feldman, S., Fonda, M., Gailhanou, M., Ma, H., Ming, D.W., Morris, R.V., Sarrazin, P., Stolper, E., Treiman, A., Yen, A., 2012. Characterization and calibration of the CheMin mineralogical instrument on Mars Science Laboratory. Space Sci. Rev. 170, 341–399. https://doi.org/10.1007/s11214-012-9905-1.

Borlina, C.S., Ehlmann, B.L., Kite, E.S., 2015. Modeling the thermal and physical evolution of Mount Sharp's sedimentary rocks, Gale Crater, Mars: implications for diagenesis on the MSL Curiosity rover traverse. J. Geophys. Res., Planets 120, 1396–1414. https://doi.org/10.1002/2015JE004799.

Bridges, J.C., Franchi, I.A., Hutchison, R., Morse, A.D., Long, J.V.P., Pillinger, C.T., 1995. Cristobalite- and tridymite-bearing clasts in Parnallee (LL3) and Farmington (L5). Meteoritics 30, 715–727. https://doi.org/10.1111/j.1945-5100.1995.tb01169.x.

Czarnecki, S., Hardgrove, C., Gasda, P.J., Gabriel, T.S.J., Starr, M., Rice, M.S., Frydenvang, J., Wiens, R.C., Rapin, W., Nikiforov, S., Lisov, D., Litvak, M., Calef, F., Gengl, H., Newsom, H., Thompson, L., Nowicki, S., 2020a. Identification and description of a silicic volcaniclastic layer in Gale crater, Mars, using active neutron interrogation. J. Geophys. Res., Planets 125, e2019JE006180.

Czarnecki, S., Hardgrove, C., Gasda, P.J., Gabriel, T.S.J., Starr, M., Rice, M.S., Frydenvang, J., Wiens, R.C., Rapin, W., Nikiforov, S., Lisov, D., Litvak, M., Calef, F., Gengl, H., Newsom, H., Thompson, L., Nowicki, S., 2020b. Identification and description of a silicic volcaniclastic layer in Gale crater, Mars, using active neutron interrogation. J. Geophys. Res., Planets 125, e2019JE006180.

Deer, W.A., Howie, R.A., Zussman, J., 2013. An Introduction to the Rock-Forming Minerals. Mineralogical Society of Great Britain and Ireland.

Dollase, W.A., Baur, W.H., 1976. The superstructure of meteoritic low tridymite solved by computer simulation. Am. Mineral. 61, 971–978.

Dollase, W.A., Cliff, R.A., Wetherill, G.W., 1971. Note on tridymite in rock 12021. In: Proceedings of the Lunar and Planetary Science Conference. Presented at the Lunar and Planetary Science Conference, p. 141.

Dove, P.M., Rlmstidt, J.D., 1994. SILICA-WATER INTERACTIONS, Silica. De Gruyter. Chapter 8.

Eversull, L.G., Ferrell, R.E., 2008. Disordered silica with tridymite-like structure in the Twiggs clay. Am. Mineral. 93, 565–572. https://doi.org/10.2138/am.2008.2603.

Frydenvang, J., Gasda, P.J., Hurowitz, J.A., Grotzinger, J.P., Wiens, R.C., Newsom, H.E., Edgett, K.S., Watkins, J., Bridges, J.C., Maurice, S., Fisk, M.R., Johnson, J.R., Rapin, W., Stein, N.T., Clegg, S.M., Schwenzer, S.P., Bedford, C.C., Edwards, P., Mangold, N., Cousin, A., Anderson, R.B., Payré, V., Vaniman, D., Blake, D.F., Lanza, N.L., Gupta, S., Van Beek, J., Sautter, V., Meslin, P.-Y., Rice, M., Milliken, R., Gellert, R., Thompson, L., Clark, B.C., Sumner, D.Y., Fraeman, A.A., Kinch, K.M., Madsen, M.B., Mitrofanov, I.G., Jun, I., Calef, F., Vasavada, A.R., 2017. Diagenetic silica enrichment and late-stage groundwater activity in Gale crater, Mars: Silica Enriching Diagenesis, Gale, Mars. Geophys. Res. Lett. 44, 4716–4724. https://doi.org/10.1002/2017GL073323.

Ganino, C., Libourel, G., Bernard, A., 2019. Fumarolic incrustations at Kudryavy volcano (Kamchatka) as a guideline for high-temperature (>850 °C) extinct hydrothermal systems. J. Volcanol. Geotherm. Res. 376, 75–85. https://doi.org/10.1016/j.jvolgeores.2019.03.020.

Getahun, A., Reed, M.H., Symonds, R., 1996. Mount St. Augustine volcano fumarole wall rock alteration: mineralogy, zoning, composition and numerical models of its formation process. J. Volcanol. Geotherm. Res. 71, 73–107. https://doi.org/10.1016/0377-0273(95)00071-2.

Ghiorso, M.S., Sack, R.O., 1995. Chemical mass transfer in magmatic processes IV. A revised and internally consistent thermodynamic model for the interpolation and extrapolation of liquid-solid equilibria in magmatic systems at elevated temperatures and pressures. Contrib. Mineral. Petrol. 119, 197–212. https://doi.org/10.1007/BF00307281.

Grotzinger, J.P., Gupta, S., Malin, M.C., Rubin, D.M., Schieber, J., Siebach, K., Sumner, D.Y., Stack, K.M., Vasavada, A.R., Arvidson, R.E., Calef, F., Edgar, L., Fischer, W.F., Grant, J.A., Griffes, J., Kah, L.C., Lamb, M.P., Lewis, K.W., Mangold, N., Minitti, M.E., Palucis, M., Rice, M., Williams, R.M.E., Yingst, R.A., Blake, D., Blaney, D., Conrad, P., Crisp, J., Dietrich, W.E., Dromart, G., Edgett, K.S., Ewing, R.C., Gellert, R., Hurowitz, J.A., Kocurek, G., Mahaffy, P., McBride, M.J., McLennan, S.M., Mischna, M., Ming, D., Milliken, R., Newsom, H., Oehler, D., Parker, T.J., Vaniman, D., Wiens, R.C., Wilson, S.A., 2015. Deposition, exhumation, and paleoclimate of an ancient lake deposit, Gale crater, Mars. Science 350, aac7575. https://doi.org/10.1126/science.aac7575.

Gualda, G.A.R., Ghiorso, M.S., Lemons, R.V., Carley, T.L., 2012. Rhyolite-MELTS: a modified calibration of MELTS optimized for silica-rich, fluid-bearing magmatic systems. J. Petrol. 53, 875–890. https://doi.org/10.1093/petrology/egr080.

Hauber, E., Platz, T., Reiss, D., Le Deit, L., Kleinhans, M.G., Marra, W.A., de Haas, T., Carbonneau, P., 2013. Asynchronous formation of Hesperian and Amazonian-aged deltas on Mars and implications for climate: ASYNCHRONOUS DELTA FORMATION ON MARS. J. Geophys. Res., Planets 118, 1529–1544. https://doi.org/10.1002/jgre.20107.

Heled, Y., Rowe, M.C., Chambefort, I., Wilson, C.J.N., 2022. Significance of tridymite distribution during cooling and vapor-phase alteration of ignimbrites. Am. Mineral. 107, 460–475. https://doi.org/10.2138/am-2021-7814.

Hirschmann, M.M., Ghiorso, M.S., Davis, F.A., Gordon, S.M., Mukherjee, S., Grove, T.L., Krawczynski, M., Medard, E., Till, C.B., 2008. Library of Experimental Phase Relations (LEPR): a database and Web portal for experimental magmatic phase equilibria data. Geochem. Geophys. Geosyst. 9. https://doi.org/10.1029/2007GC001894.

Hoffmann, W., 1967. Gitterkonstanten und Raumgruppe von Tridymit bei 20 °C. Naturwissenschaften 54, 114. https://doi.org/10.1007/BF00640573.

Hurowitz, J.A., Grotzinger, J.P., Fischer, W.W., McLennan, S.M., Milliken, R.E., Stein, N., Vasavada, A.R., Blake, D.F., Dehouck, E., Eigenbrode, J.L., Fairén, A.G., Frydenvang, J., Gellert, R., Grant, J.A., Gupta, S., Herkenhoff, K.E., Ming, D.W., Rampe, E.B., Schmidt, M.E., Siebach, K.L., Stack-Morgan, K., Sumner, D.Y., Wiens, R.C., 2017. Redox stratification of an ancient lake in Gale crater, Mars. Science 356, eaah6849. https://doi.org/10.1126/science.aah6849.

Jackson, J.C., Horton, J.W., Chou, I.-M., Belkin, H.E., 2011. Monoclinic tridymite in clast-rich impact melt rock from the Chesapeake Bay impact structure. Am. Mineral. 96, 81–88. https://doi.org/10.2138/am.2011.3589.

John, D.A., Sisson, T.W., Breit, G.N., Rye, R.O., Vallance, J.W., 2008. Characteristics, extent and origin of hydrothermal alteration at Mount Rainier Volcano, Cascades Arc, USA: implications for debris-flow hazards and mineral deposits. J. Volcanol. Geotherm. Res. 175, 289–314. https://doi.org/10.1016/j.jvolgeores.2008.04.004.

Kawai, K., Matsumoto, T., Kihara, K., Sakurai, K., 1978. The first finding of monoclinic tridymite in terrestrial volcanic rocks. Mineral. J. 9, 231–235. https://doi.org/10.2465/minerj.9.231.

Kerber, L., Forget, F., Madeleine, J.-B., Wordsworth, R., Head, J.W., Wilson, L., 2013. The effect of atmospheric pressure on the dispersal of pyroclasts from martian volcanoes. Icarus 223, 149–156. https://doi.org/10.1016/j.icarus.2012.11.037.

Kihara, K., 1978. Thermal change in unit-cell dimensions, and a hexagonal structure of tridymite. Z. Kristallogr. (Crystalline Materials) 148, 237–254. https://doi.org/10.1524/zkri-1978-3-406.

Kite, E.S., Lewis, K.W., Lamb, M.P., Newman, C.E., Richardson, M.I., 2013. Growth and form of the mound in Gale Crater, Mars: slope wind enhanced erosion and transport. Geology 41, 543–546. https://doi.org/10.1130/G33909.1.

Kushiro, I., 1975. On the nature of silicate melt and its significance in magma genesis; regularities in the shift of the liquidus boundaries involving olivine, pyroxene, and silica minerals. Am. J. Sci. 275, 411–431. https://doi.org/10.2475/ajs.275.4.411.

Larsen, R.B., Tegner, C., 2006. Pressure conditions for the solidification of the Skaergaard intrusion: eruption of East Greenland flood basalts in less than 300,000 years. Lithos Magmat. Tecton. Greenl. Rifts 92, 181–197. https://doi.org/10.1016/j.lithos.2006.03.032.

Le Deit, L., Mangold, N., Forni, O., Cousin, A., Lasue, J., Schröder, S., Wiens, R.C., Sumner, D., Fabre, C., Stack, K.M., Anderson, R.B., Blaney, D., Clegg, S., Dromart, G., Fisk, M., Gasnault, O., Grotzinger, J.P., Gupta, S., Lanza, N., Le Mouélic, S., Maurice, S., McLennan, S.M., Meslin, P.-Y., Nachon, M., Newsom, H., Payré, V., Rapin, W., Rice, M., Sautter, V., Treiman, A.H., 2016. The potassic sedimentary rocks in Gale Crater, Mars, as seen by ChemCam on board Curiosity. J. Geophys. Res., Planets 121, 2015JE004987. https://doi.org/10.1002/2015JE004987.

Malin, M.C., 2000. Sedimentary rocks of early Mars. Science 290, 1927–1937. https://doi.org/10.1126/science.290.5498.1927.

Mas, G., Bengochea, L., Mas, L., de Energía, S., 2000. Hydrothermal alteration at El Humazo geothermal area, Domuyo volcano, Argentina. In: Undefined, Presented at the Proceedings of the World Geothermal Congress, Proceedings of the World Geothermal Congress, pp. 14313–1418.

Mason, B., 1972. Lunar tridymite and cristobalite. Am. Mineral. 57, 1530–1535.

McKay, D.S., Clanton, U.S., Morrison, D.A., 1972. Vapor phase crystallization in Apollo 14 breccia 3, 739.

Michalski, J.R., Bleacher, J.E., 2013. Supervolcanoes within an ancient volcanic province in Arabia Terra, Mars. Nature 502, 47–52. https://doi.org/10.1038/nature12482.

Michalski, J.R., Kraft, M.D., Diedrich, T., Sharp, T.G., Christensen, P.R., 2003. Thermal emission spectroscopy of the silica polymorphs and considerations for remote sensing of Mars. Geophys. Res. Lett. 30. https://doi.org/10.1029/2003GL018354.

Milliken, R.E., Grotzinger, J.P., Thomson, B.J., 2010. Paleoclimate of Mars as captured by the stratigraphic record in Gale Crater. Geophys. Res. Lett. 37. https://doi.org/10.1029/2009GL041870.

Morris, R.V., Vaniman, D.T., Blake, D.F., Gellert, R., Chipera, S.J., Rampe, E.B., Ming, D.W., Morrison, S.M., Downs, R.T., Treiman, A.H., Yen, A.S., Grotzinger, J.P., Achilles, C.N., Bristow, T.F., Crisp, J.A., Des Marais, D.J., Farmer, J.D., Fendrich, K.V., Frydenvang, J., Graff, T.G., Morookian, J.-M., Stolper, E.M., Schwenzer, S.P., 2016. Silicic volcanism on Mars evidenced by tridymite in high-SiO2 sedimentary rock at Gale crater. Proc. Natl. Acad. Sci. 113, 7071–7076. https://doi.org/10.1073/pnas.1607098113.

Morrison, S.M., Downs, R.T., Blake, D.F., Prabhu, A., Eleish, A., Vaniman, D.T., Ming, D.W., Rampe, E.B., Hazen, R.M., Achilles, C.N., Treiman, A.H., Yen, A.S., Morris, R.V., Bristow, T.F., Chipera, S.J., Sarrazin, P.C., Fendrich, K.V., Morookian, J.M., Farmer, J.D., Marais, D.J.D., Craig, P.I., 2018. Relationships between unit-cell parameters and composition for rock-forming minerals on Earth, Mars, and other extraterrestrial bodies. Am. Mineral. 103, 848–856. https://doi.org/10.2138/am-2018-6123.

Nukui, A., Nakazawa, H., 1978. Thermal changes in monoclinic tridymite. Am. Mineral. 63, 1252–1259.

Payré, V., Siebach, K.L., Dasgupta, R., Udry, A., Rampe, E.B., Morrison, S.M., 2020. Constraining ancient magmatic evolution on Mars using crystal chemistry of detrital igneous minerals in the sedimentary Bradbury group, Gale crater, Mars. J. Geophys. Res., Planets 125, e2020JE006467. https://doi.org/10.1029/2020JE006467.

Pryde, A.K.A., Dove, M.T., 1998. On the sequence of phase transitions in tridymite. Phys. Chem. Miner. 26, 171–179. https://doi.org/10.1007/s002690050174.

Rampe, E.B., Blake, D.F., Bristow, T.F., Ming, D.W., Vaniman, D.T., Morris, R.V., Achilles, C.N., Chipera, S.J., Morrison, S.M., Tu, V.M., Yen, A.S., Castle, N., Downs, G.W., Downs, R.T., Grotzinger, J.P., Hazen, R.M., Treiman, A.H., Peretyazhko, T.S., Des Marais, D.J., Walroth, R.C., Craig, P.I., Crisp, J.A., Lafuente, B., Morookian, J.M., Sarrazin, P.C., Thorpe, M.T., Bridges, J.C., Edgar, L.A., Fedo, C.M., Freissinet, C., Gellert, R., Mahaffy, P.R., Newsom, H.E., Johnson, J.R., Kah, L.C., Siebach, K.L., Schieber, J., Sun, V.Z., Vasavada, A.R., Wellington, D., Wiens, R.C., 2020. Mineralogy and geochemistry of sedimentary rocks and eolian sediments in Gale crater, Mars: a review after six Earth years of exploration with Curiosity. Geochemistry 80, 125605. https://doi.org/10.1016/j.chemer.2020.125605.

Rampe, E.B., Ming, D.W., Blake, D.F., Bristow, T.F., Chipera, S.J., Grotzinger, J.P., Morris, R.V., Morrison, S.M., Vaniman, D.T., Yen, A.S., Achilles, C.N., Craig, P.I., Des Marais, D.J., Downs, R.T., Farmer, J.D., Fendrich, K.V., Gellert, R., Hazen, R.M., Kah, L.C., Morookian, J.M., Peretyazhko, T.S., Sarrazin, P., Treiman, A.H., Berger, J.A., Eigenbrode, J., Fairén, A.G., Forni, O., Gupta, S., Hurowitz, J.A., Lanza, N.L., Schmidt, M.E., Siebach, K., Sutter, B., Thompson, L.M., 2017. Mineralogy of an ancient lacustrine mudstone succession from the Murray formation, Gale crater, Mars. Earth Planet. Sci. Lett. 471, 172–185. https://doi.org/10.1016/j.epsl.2017.04.021.

Robie, R.A., Hemingway, B.S., Fisher, J.R., 1978. Thermodynamic properties of minerals and related substances at 298. 15 K and 1 bar (10/sup 5/pascals) pressure and at higher temperatures (No. USGS-BULL-1452). Geological Survey, Washington, DC (USA).

Romans, B.W., Castelltort, S., Covault, J.A., Fildani, A., Walsh, J.P., 2016. Environmental signal propagation in sedimentary systems across timescales. Earth-Sci. Rev. 153, 7–29. https://doi.org/10.1016/j.earscirev.2015.07.012. Source-to-Sink Systems: Sediment & Solute Transfer on the Earth Surface.

Roy, P.D., Caballero, M., Lozano, R., Pi, T., Morton, O., 2009a. Late Pleistocene-Holocene geochemical history inferred from Lake Tecocomulco sediments, Basin of Mexico, Mexico. Geochem. J. 43, 49–64. https://doi.org/10.2343/geochemj.1.0006.

Roy, P.D., Caballero, M., Lozano, R., Pi, T., Morton, O., 2009b. Late Pleistocene-Holocene geochemical history inferred from Lake Tecocomulco sediments, Basin of Mexico, Mexico. Geochem. J. 43, 49–64. https://doi.org/10.2343/geochemj.1.0006.

Rudnick, R.L., 2018. Earth's continental crust. In: White, W.M. (Ed.), Encyclopedia of Geochemistry: A Comprehensive Reference Source on the Chemistry of the Earth. Springer International Publishing, Cham, pp. 392–418.

Ruff, S.W., Farmer, J.D., 2016. Silica deposits on Mars with features resembling hot spring biosignatures at El Tatio in Chile. Nat. Commun. 7, 13554. https://doi.org/10.1038/ncomms13554.

Sautter, V., Toplis, M.J., Beck, P., Mangold, N., Wiens, R., Pinet, P., Cousin, A., Maurice, S., LeDeit, L., Hewins, R., Gasnault, O., Quantin, C., Forni, O., Newsom, H., Meslin, P.-Y., Wray, J., Bridges, N., Payré, V., Rapin, W., Le Mouélic, S., 2016. Magmatic complexity on early Mars as seen through a combination of orbital, in-situ and meteorite data. Lithos 254–255, 36–52. https://doi.org/10.1016/j.lithos.2016.02.023.

Sautter, V., Toplis, M.J., Wiens, R.C., Cousin, A., Fabre, C., Gasnault, O., Maurice, S., Forni, O., Lasue, J., Ollila, A., Bridges, J.C., Mangold, N., Le Mouélic, S., Fisk, M., Meslin, P.-Y., Beck, P., Pinet, P., Le Deit, L., Rapin, W., Stolper, E.M., Newsom, H., Dyar, D., Lanza, N., Vaniman, D., Clegg, S., Wray, J.J., 2015. In situ evidence for continental crust on early Mars. Nat. Geosci. 8, 605–609. https://doi.org/10.1038/ngeo2474.

Schneider, H., Wohlleben, K., Majdic, A., 1980. Incorporation of impurities in tridymites from a used silica brick. Mineral. Mag. 43, 879–883. https://doi.org/10.1180/minmag.1980.043.331.10.

Siebach, K.L., Baker, M.B., Grotzinger, J.P., McLennan, S.M., Gellert, R., Thompson, L.M., Hurowitz, J.A., 2017. Sorting out compositional trends in sedimentary rocks of the Bradbury group (Aeolis Palus), Gale crater, Mars. J. Geophys. Res., Planets 122, 295–328. https://doi.org/10.1002/2016JE005195.

Smith, D.K., 1998. Opal, cristobalite, and tridymite: noncrystallinity versus crystallinity, nomenclature of the silica minerals and bibliography. Powder Diffr. 13, 2–19. https://doi.org/10.1017/S0885715600009696.

Smith, P.M., Asimow, P.D., 2005. Adiabat_1ph: a new public front-end to the MELTS, pMELTS, and pHMELTS models. Geochem. Geophys. Geosyst. 6. https://doi.org/10.1029/2004GC000816.

Stack, K.M., Grotzinger, J.P., Lamb, M.P., Gupta, S., Rubin, D.M., Kah, L.C., Edgar, L.A., Fey, D.M., Hurowitz, J.A., McBride, M., Rivera-Hernández, F., Sumner, D.Y., Beek, J.K.V., Williams, R.M.E., Yingst, R.A., 2019. Evidence for plunging river plume deposits in the Pahrump Hills member of the Murray formation, Gale crater, Mars. Sedimentology 66, 1768–1802. https://doi.org/10.1111/sed.12558.

Taylor, S.R., McLennan, S., 2009. Planetary Crusts: Their Composition, Origin and Evolution. Cambridge University Press, Cambridge.

Thomson, B.J., Bridges, N.T., Milliken, R., Baldridge, A., Hook, S.J., Crowley, J.K., Marion, G.M., de Souza Filho, C.R., Brown, A.J., Weitz, C.M., 2011. Constraints on the origin and evolution of the layered mound in Gale Crater, Mars using Mars Reconnaissance Orbiter data. Icarus 214, 413–432. https://doi.org/10.1016/j.icarus.2011.05.002.

Thomson, B.J., Buczkowski, D.L., Crumpler, L.S., Seelos, K.D., Fassett, C.I., 2019. How much of the sediment in Gale crater's central mound was fluvially transported? Geophys. Res. Lett. 46, 5092–5099. https://doi.org/10.1029/2018GL081727.

Udry, A., Gazel, E., McSween, H.Y., 2018. Formation of evolved rocks at Gale crater by crystal fractionation and implications for Mars crustal composition. J. Geophys. Res., Planets 123, 1525–1540. https://doi.org/10.1029/2018JE005602.

Vaniman, D.T., Bish, D.L., Ming, D.W., Bristow, T.F., Morris, R.V., Blake, D.F., Chipera, S.J., Morrison, S.M., Treiman, A.H., Rampe, E.B., Rice, M., Achilles, C.N., Grotzinger, J.P., McLennan, S.M., Williams, J., Bell, J.F., Newsom, H.E., Downs, R.T., Maurice, S., Sarrazin, P., Yen, A.S., Morookian, J.M., Farmer, J.D., Stack, K., Milliken, R.E., Ehlmann, B.L., Sumner, D.Y., Berger, G., Crisp, J.A., Hurowitz, J.A., Anderson, R., Des Marais, D.J., Stolper, E.M., Edgett, K.S., Gupta, S., Spanovich, N., Alves Verdasca, J.A., Anderson, R., Archer, D., Armiens-Aparicio, C., Arvidson, R., Atlaskin, E., Atreya, S., Aubrey, A., Baker, B., Baker, M., Balic-Zunic, T., Baratoux, D., Baroukh, J., Barraclough, B., Bean, K., Beegle, L., Behar, A., Bender, S., Benna, M., Bentz, J., Berger, J., Berman, D., Blanco Avalos, J.J., Blaney, D., Blank, J., Blau, H., Bleacher, L., Boehm, E., Botta, O., Bottcher, S., Boucher, T., Bower, H., Boyd, N., Boynton, B., Breves, E., Bridges, J., Bridges, N., Brinckerhoff, W., Brinza, D., Brunet, C., Brunner, A., Brunner, W., Buch, A., Bullock, M., Burmeister, S., Cabane, M., Calef, F., Cameron, J., Campbell, J.I., Cantor, B., Caplinger, M., Caride Rodriguez, J., Carmosino, M., Carrasco Blazquez, I., Charpentier, A., Choi, D., Clark, B., Clegg, S., Cleghorn, T., Cloutis, E., Cody, G., Coll, P., Conrad, P., Coscia, D., Cousin, A., Cremers, D., Cros, A., Cucinotta, F., d'Uston, C., Davis, S., Day, M.K., de la Torre Juarez, M., DeFlores, L., DeLapp, D., DeMarines, J., Dietrich, W., Dingler, R., Donny, C., Drake, D., Dromart, G., Dupont, A., Duston, B., Dworkin, J., Dyar, M.D., Edgar, L., Edwards, C., Edwards, L., Ehresmann, B., Eigenbrode, J., Elliott, B., Elliott, H., Ewing, R., Fabre, C., Fairen, A., Farley, K., Fassett, C., Favot, L., Fay, D., Fedosov, F., Feldman, J., Feldman, S., Fisk, M., Fitzgibbon, M., Flesch, G., Floyd, M., Fluckiger, L., Forni, O., Fraeman, A., Francis, R., Francois, P., Franz, H., Freissinet, C., French, K.L., Frydenvang, J., Gaboriaud, A., Gailhanou, M., Garvin, J., Gasnault, O., Geffroy, C., Gellert, R., Genzer, M., Glavin, D., Godber, A., Goesmann, F., Goetz, W.,

Golovin, D., Gomez Gomez, F., Gomez-Elvira, J., Gondet, B., Gordon, S., Gorevan, S., Grant, J., Griffes, J., Grinspoon, D., Guillemot, P., Guo, J., Guzewich, S., Haberle, R., Halleaux, D., Hallet, B., Hamilton, V., Hardgrove, C., Harker, D., Harpold, D., Harri, A.-M., Harshman, K., Hassler, D., Haukka, H., Hayes, A., Herkenhoff, K., Herrera, P., Hettrich, S., Heydari, E., Hipkin, V., Hoehler, T., Hollingsworth, J., Hudgins, J., Huntress, W., Hviid, S., Iagnemma, K., Indyk, S., Israel, G., Jackson, R., Jacob, S., Jakosky, B., Jensen, E., Jensen, J.K., Johnson, J., Johnson, M., Johnstone, S., Jones, A., Jones, J., Joseph, J., Jun, I., Kah, L., Kahanpaa, H., Kahre, M., Karpushkina, N., Kasprzak, W., Kauhanen, J., Keely, L., Kemppinen, O., Keymeulen, D., Kim, M.-H., Kinch, K., King, P., Kirkland, L., Kocurek, G., Koefoed, A., Kohler, J., Kortmann, O., Kozyrev, A., Krezoski, J., Krysak, D., Kuzmin, R., Lacour, J.L., Lafaille, V., Langevin, Y., Lanza, N., Lasue, J., Le Mouelic, S., Lee, E.M., Lee, Q.-M., Lees, D., Lefavor, M., Lemmon, M., Malvitte, A.L., Leshin, L., Leveille, R., Lewin-Carpintier, E., Lewis, K., Li, S., Lipkaman, L., Little, C., Litvak, M., Lorigny, E., Lugmair, G., Lundberg, A., Lyness, E., Madsen, M., Mahaffy, P., Maki, J., Malakhov, A., Malespin, C., Malin, M., Mangold, N., Manhes, G., Manning, H., Marchand, G., Marin Jimenez, M., Martin Garcia, C., Martin, D., Martin, M., Martinez-Frias, J., Martin-Soler, J., Martin-Torres, F.J., Mauchien, P., McAdam, A., McCartney, E., McConnochie, T., McCullough, E., McEwan, I., McKay, C., McNair, S., Melikechi, N., Meslin, P.-Y., Meyer, M., Mezzacappa, A., Miller, H., Miller, K., Minitti, M., Mischna, M., Mitrofanov, I., Moersch, J., Mokrousov, M., Molina Jurado, A., Moores, J., Mora-Sotomayor, L., Mueller-Mellin, R., Muller, J.-P., Munoz Caro, G., Nachon, M., Navarro Lopez, S., MSL Science Team, Agard, C., Navarro-Gonzalez, R., Nealson, K., Nefian, A., Nelson, T., Newcombe, M., Newman, C., Nikiforov, S., Niles, P., Nixon, B., Noe Dobrea, E., Nolan, T., Oehler, D., Ollila, A., Olson, T., Owen, T., de Pablo Hernandez, M.A., Paillet, A., Pallier, E., Palucis, M., Parker, T., Parot, Y., Patel, K., Paton, M., Paulsen, G., Pavlov, A., Pavri, B., Peinado-Gonzalez, V., Pepin, R., Peret, L., Perez, R., Perrett, G., Peterson, J., Pilorget, C., Pinet, P., Pla-Garcia, J., Plante, I., Poitrasson, F., Polkko, J., Popa, R., Posiolova, L., Posner, A., Pradler, I., Prats, B., Prokhorov, V., Purdy, S.W., Raaen, E., Radziemski, L., Rafkin, S., Ramos, M., Raulin, F., Ravine, M., Reitz, G., Renno, N., Richardson, M., Robert, F., Robertson, K., Rodriguez Manfredi, J.A., Romeral-Planello, J.J., Rowland, S., Rubin, D., Saccoccio, M., Salamon, A., Sandoval, J., Sanin, A., Sans Fuentes, S.A., Saper, L., Sautter, V., Savijarvi, H., Schieber, J., Schmidt, M., Schmidt, W., Scholes, D.D., Schoppers, M., Schroder, S., Schwenzer, S., Sebastian Martinez, E., Sengstacken, A., Shterts, R., Siebach, K., Siili, T., Simmonds, J., Sirven, J.-B., Slavney, S., Sletten, R., Smith, M., Sobron Sanchez, P., Spray, J., Squyres, S., Stalport, F., Steele, A., Stein, T., Stern, J., Stewart, N., Stipp, S.L.S., Stoiber, K., Sucharski, B., Sullivan, R., Summons, R., Sun, V., Supulver, K., Sutter, B., Szopa, C., Tan, F., Tate, C., Teinturier, S., ten Kate, I., Thomas, P., Thompson, L., Tokar, R., Toplis, M., Torres Redondo, J., Trainer, M., Tretyakov, V., Urqui-O'Callaghan, R., Van Beek, J., Van Beek, T., VanBommel, S., Varenikov, A., Vasavada, A., Vasconcelos, P., Vicenzi, E., Vostrukhin, A., Voytek, M., Wadhwa, M., Ward, J., Webster, C., Weigle, E., Wellington, D., Westall, F., Wiens, R.C., Wilhelm, M.B., Williams, A., Williams, R., Williams, R.B.M., Wilson, M., Wimmer-Schweingruber, R., Wolff, M., Wong, M., Wray, J., Wu, M., Yana, C., Yingst, A., Zeitlin, C., Zimdar, R., Zorzano Mier, M.-P., 2014. Mineralogy of a Mudstone at Yellowknife Bay, Gale Crater, Mars. Science 343, 1243480. https://doi.org/10.1126/science.1243480.

White, W.M., Klein, E.M., 2014. Composition of the oceanic crust. In: Treatise on Geochemistry. Elsevier, pp. 457–496.

Xirouchakis, D., Draper, D.S., Schwandt, C.S., Lanzirotti, A., 2002. Crystallization conditions of Los Angeles, a basaltic Martian meteorite. Geochim. Cosmochim. Acta 66, 1867–1880. https://doi.org/10.1016/S0016-7037(01)00892-4.

Yen, A.S., Morris, R.V., Ming, D.W., Schwenzer, S.P., Sutter, B., Vaniman, D.T., Treiman, A.H., Gellert, R., Achilles, C.N., Berger, J.A., Blake, D.F., Boyd, N.I., Bristow, T.F., Chipera, S., Clark, B.C., Craig, P.I., Downs, R.T., Franz, H.B., Gabriel, T., McAdam, A.C., Morrison, S.M., O'Connell-Cooper, C.D., Rampe, E.B., Schmidt, M.E., Thompson, L.M., VanBommel, S.J., 2021. Formation of tridymite and evidence for a hydrothermal history at Gale crater, Mars. J. Geophys. Res., Planets 126, e2020JE006569. https://doi.org/10.1029/2020JE006569.